Bioactive Materials 31 (2024) 119–135

Contents lists available at ScienceDirect

Bioactive Materials

journal homepage: www.keaipublishing.com/en/journals/bioactive-materials

# Development and preclinical evaluation of multifunctional hydrogel for precise thermal protection during thermal ablation

Bowen Zheng [a,1], Peng Zhang [b,1], Qijun Lv [a], Tao Wu [a], Yadong Liu [b], Junjie Tang [b], Yanping Ma [a], Lili Cheng [b], Langtao Xu [b], Yizhen Wang [a], Yifan Xue [b], Jie Liu [b,*], Jie Ren [a,**]

[a] Department of Medical Ultrasonics, The Third Affiliated Hospital of Sun Yat-sen University, Guangdong Province Key Laboratory of Hepatology Research, Multiple Disciplinary Team Center of Thyroid Diseases, No. 600, Tianhe Road, Guangzhou, Guangdong, 510630, PR China
[b] School of Biomedical Engineering, Shenzhen Campus of Sun Yat-sen University, No.66, Gongchang Road, Shenzhen, Guangdong, 518107, PR China

ARTICLE INFO

*Keywords:*
Thermal ablation
Hydrogels
Protection
Neuroprotection
Hydrodissection

ABSTRACT

Image-guided thermal ablation (TA), which is less invasive, has been widely applied for treating various kinds of tumors. However, TA still poses the potential risk of thermal damage to sensitive tissue nearby. Therefore, an adjunctive thermoprotective hydrodissection technique with constant injection of 5% glucose (5% Glu) has currently been adopted for clinical application, but this may be hazardous to humans. In this study, a multifunctional hyaluronic acid-based hydrogel (HA-Dc) was developed for hydrodissection. Compared with 5% Glu (the most clinically used solution) and the previously reported F127 hydrogel, the HA-Dc hydrogel was studied *in vitro* in a porcine liver model and *in vivo* in a rabbit model and showed good injectability and better tissue retention, stability, and thermoprotective properties throughout the TA procedure. Furthermore, in the preclinical evaluation in a *Macaca fascicularis (M. fascicularis)* model, HA-Dc showed excellent performance in terms of stricter neuroprotection compared with 5% Glu. In addition, the HA-Dc hydrogel with good biocompatibility and controllable degradation behavior *in vivo* could be a promising platform for thermal protection during clinical TA procedures.

## 1. Introduction

Image-guided thermal ablation (TA) has been increasingly applied for treating benign and malignant tumors in a wide range of organs [1,2], including the liver [3,4], lung [5,6], kidney [7], bone [8], thyroid [9,10], adrenal [11,12], and soft tissue [13,14]. TA produces high temperatures locally to induce irreversible cell injury, ultimately tumor apoptosis, and coagulative necrosis [2,15,16]. When performed percutaneously, TA is less invasive and has fewer complications with a faster recovery than traditional open surgery [17–23]. Although TA procedures are well tolerated, they still carry the risk of thermal injury to sensitive structures in the vicinity of the ablation zone that should not be ablated, such as nerves [24–27], bile ducts, major blood vessels, the diaphragm, the body wall, and the gastrointestinal tract [28–30]. Damage to these structures can cause complications ranging from those that are minor, such as discomfort and pain, to those that are major, such as bowel perforation, nerve deficit and death. Therefore, adjunctive thermoprotective techniques have been developed to reduce the risk of thermal injury to critical structures nearby and improve procedural safety and efficacy, including hydrodissection [31–34], carbodissection [35,36], balloon interposition [37], and probe torquing [38].

The most widely used procedure for this purpose is hydrodissection, which has been used in clinical practice for over a decade [33,34,39]. Hydrodissection is a technique that consists of injecting fluids between the target zone and susceptible structures to provide a physical and thermal barrier during the TA procedure. Solutions such as 5% glucose (5% Glu) and normal saline are the most clinically used and have been shown to be effective in reducing complications from thermal injury [33,34,40]. However, these liquids are both highly mobile and easily disperse away from the target site and quickly absorbable, potentially compromising their protective effects during the TA procedure [41]. As a result, a relatively large amount of liquid or continuous liquid injection

Peer review under responsibility of KeAi Communications Co., Ltd.
* Corresponding author.
** Corresponding author.
*E-mail addresses:* liujie56@mail.sysu.edu.cn (J. Liu), renjie@mail.sysu.edu.cn (J. Ren).
[1] The authors contributed equally to this work.

https://doi.org/10.1016/j.bioactmat.2023.08.010
Received 5 June 2023; Received in revised form 7 August 2023; Accepted 8 August 2023

is often required to ensure adequate protection [42,43], which can be hazardous to human safety by causing unintended bleeding, or life-threatening hydroelectrolytic disorders [44,45].

To solve the clinical limitations of 5% Glu, researchers have focused on alternative biomaterials with relatively higher viscosities but comparable thermal protection [46–50]. Thermoprotective hydrogels have been developed for this purpose, and their feasibility as an alternative to conventional liquids has been evaluated [47,49,50]. For example, a thermosensitive poloxamer 407 hydrogel (F127) was studied and shown to create a more durable barrier between the tumor and surrounding organ(s) after injection of a reduced volume compared with the liquid volume injected while still protecting nontarget tissues from thermal damage during the TA procedure [47,51,52]. However, previous work found that the F127 barrier needed to be thicker than the 5% Glu barrier [47,51] for comparable thermal protection due to its main mechanism of heat conduction rather than convection, which is the mechanism of 5% Glu [53]. This indicates that thermal protection with F127 depends on a sufficiently large separation distance, which may greatly limit its application in narrow spaces (e.g., the neck and bone) and more thermosensitive tissues (e.g., nerves). In addition, F127 is a nonbiodegradable polymer that takes a few days to be excreted through the urinary system [54], and a prolonged stay *in vivo* would easily cause a metabolic burden in the body.

In this study, we attempted to develop a multifunctional hydrogel to overcome the disadvantages of previously developed materials for hydrodissection (Fig. 1). This new hydrogel should first have good retention so that it can remain at the injection site and maintain sufficient displacement of the vulnerable structures throughout the ablation procedure. Second, and most importantly, the hydrogel should provide adequate thermal protection, even for more thermosensitive structures such as nerves, which have a lower temperature threshold for induced thermal injury (42 °C) [55,56] than other major organs (over 60 °C) [58,59]. Third, the hydrogel should also have good biocompatibility and controllable degradation *in vivo* within a finite period. Herein, a hydrogel composed of hyaluronic acid grafted with dimethyl cysteine (HA-Dc) was designed for precise neuroprotection during the TA procedure. The tissue retention, thermal protection, and biocompatibility of the HA-Dc hydrogel were evaluated using radiofrequency ablation (RFA) in both an *in vitro* porcine liver model and an *in vivo* rabbit model for comparison with 5% Glu and F127. Furthermore, stricter neuroprotection of hyperthermia-sensitive structures in thyroid nodules (TNs) was chosen for preclinical evaluation in a *Macaca fascicularis* model. These structures were chosen since hydrodissection is especially important in the ablation of TNs because cervical spaces are relatively narrow and contain many critical structures, and TNs are usually adjacent to important nerves. We believe that this novel hydrogel shows

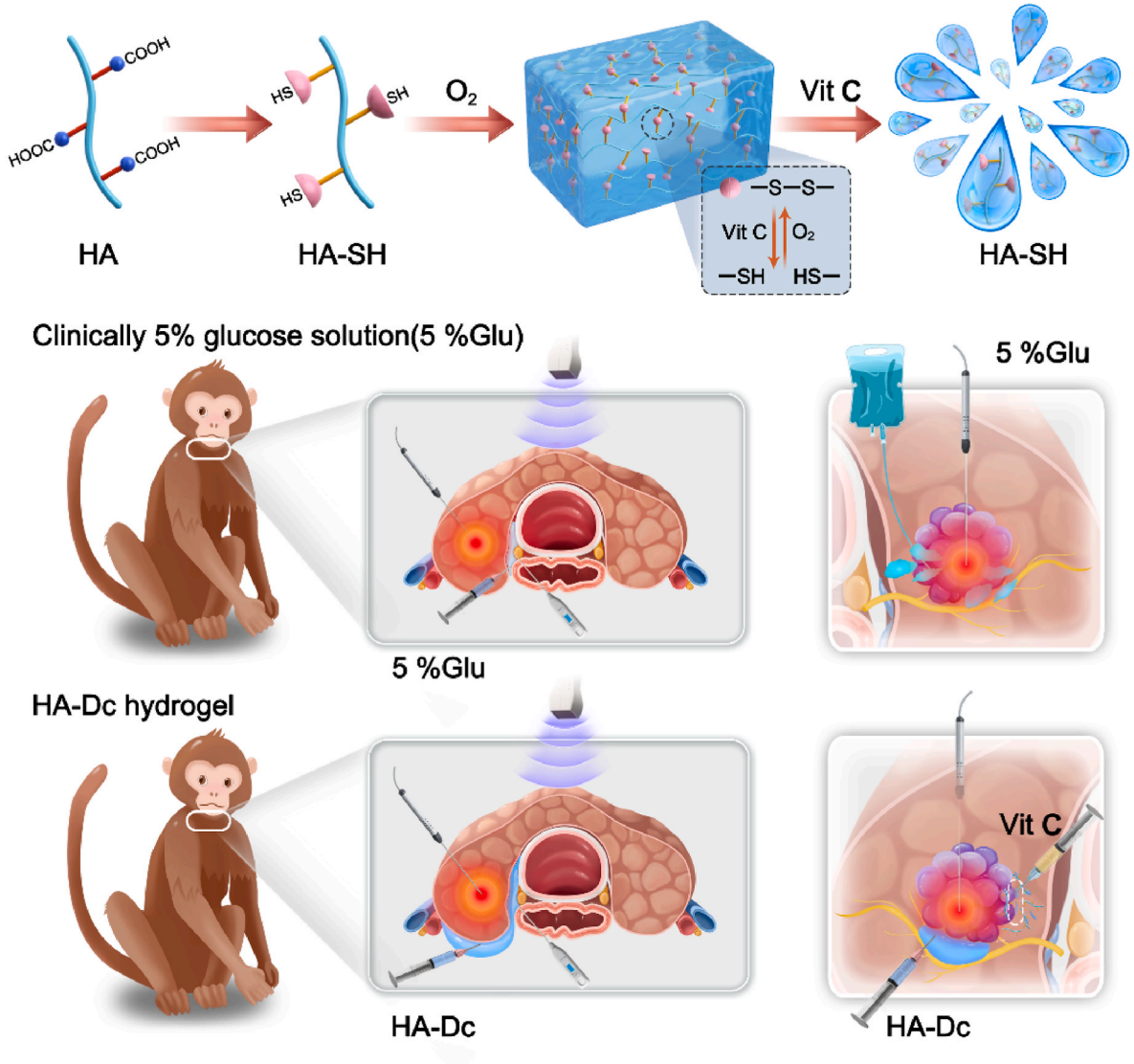


**Fig. 1.** Schematic illustration of preparation and preclinical evaluation of multifunctional HA-Dc hydrogel for precise thermal protection during thermal ablation.

excellent performance during the TA procedure and has promising potential in clinical applications.

## 2. Results and discussion

### 2.1. Preparation and characterization of the HA-Dc hydrogel

The HA-Dc hydrogel was synthesized according to the procedure shown in Fig. 2a and Fig. S1. The successful synthesis of sulfhydryl hyaluronic acid (HA-SH) modified with methyl cysteine was confirmed by $^{1}$H nuclear magnetic resonance ($^{1}$H NMR) spectroscopy. 5,5′-Dithiobis-(2-nitrobenzoic acid) (DTNB) was used to detect thiol groups. The grafting rates of HA-SH with different molecular weights ($M_w$ values) were 4.1–4.2% (Fig. S2). In Fig. 2b, the appearance of both a narrow singlet from methyl protons at $\delta$ 3.73 ppm and a singlet from thiol protons at $\delta$ 2.80 ppm of methyl cysteine confirmed the –SH modification. The absorption peak from thiol groups at 2600 $cm^{-1}$ observed by Fourier transform infrared (FTIR) spectroscopy further validated the successful grafting of HA-SH (Fig. 2c).

Scanning electron microscopy (SEM) images showed that the HA-Dc hydrogel possessed 3-dimensional porous structures, and the surface pore size increased as the $M_w$ of HA increased from 100 kDa to 300 kDa and 1200 kDa (Fig. S3). The results of rheological analysis showed that the initial viscosity of the HA-Dc hydrogel increased with increasing HA $M_w$ (Fig. 2d), suggesting that the HA-Dc hydrogel with a lower $M_w$ would be less viscous, which is beneficial for administration via injection. In addition, with increasing shear rate, the viscosities of all of the HA-Dc hydrogels with different $M_w$ values decreased, meaning that the internal structures were loose and the hydrogel possessed a shear thinning effect, which is an indication of their injectability.

The injectability of the HA-Dc hydrogel was further evaluated using an Instron tester. Measurement of the injection forces needed for HA-Dc with 100 kDa and 300 kDa HA showed that these hydrogels had better injectability (<2.5 N) than HA-Dc with 1200 kDa HA (>20.0 N),

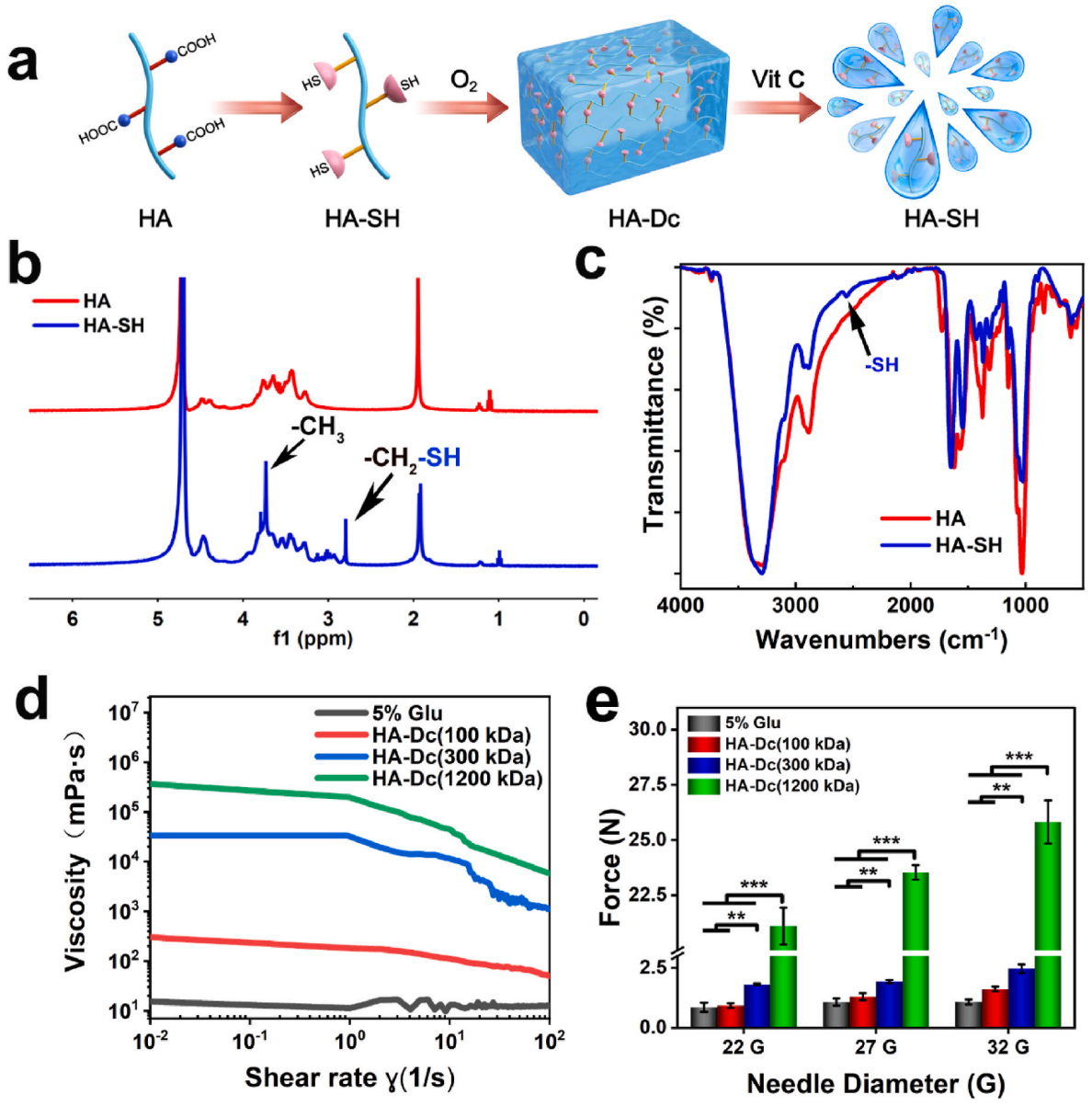


**Fig. 2.** Preparation and characterization of the HA-Dc hydrogel. **a** Schematic illustration of the preparation and decrosslinking procedure of the HA-Dc hydrogel via a chemical grafting process. **b** $^{1}$H NMR and **c** FTIR spectra for the thiol verification of HA-SH. **d** Shear thinning properties among 5% Glu and HA-Dc with different Mw. **e** The injection force of 5% Glu and HA-Dc hydrogels with different Mw of 100 kDa, 300 kDa and 1200 kDa and with different needles of 22 G, 27 G, 32 G (data are presented as the mean ± SD, n = 3, $^{**}p < 0.01$ and $^{***}p < 0.001$).

indicating that injectability could be improved by using HA with a lower $M_w$ (Fig. 2e, Fig. S4). Furthermore, the force required for injection of HA-Dc with 100 kDa and 300 kDa $M_w$ HA did not change significantly with the use of the different needles or displacements. The above results showed that the HA-Dc hydrogels with HA $M_w$ values of 100 kDa and 300 kDa possessed better injectability than the hydrogel with a HA $M_w$ of 1200 kDa. However, the local retention of the 100 kDa HA-Dc hydrogel was not satisfactory for hydrodissection due to it being a liquid, as it could not remain stable in the local environment *in vivo*. When considering retention, HA-Dc with 100 kDa HA is a liquid with high mobility, which is not conducive to remaining in the local environment *in vivo*, while HA-Dc with 300 kDa and 1200 kDa HA are colloids that can maintain a stable shape *in vivo* (Fig. S5). For comparison, the HA-Dc hydrogel with a HA $M_w$ of 300 kDa with fluid gel properties could be easily injected without blockage through the 27 G needles that are commonly used in clinical practice, with an injection force of 2.46 ± 0.18 N. Additionally, we explored the rheological properties of hydrogels with different concentrations: 0.5%, 1%, and 2% (Figs. S6 and S7). The rheological analysis revealed that the 1% and 2% HA-Dc hydrogels exhibited a gel-like state with favorable G' (storage modulus) and G'' (loss modulus), suggesting their potential for prolonged *in vivo* retention. The injectability experiment revealed that the injection pressure of the 2% HA-Dc hydrogel exceeded 20.0 N (28.6 ± 2.0 N), rendering it unsuitable for injection. Furthermore, the G′, G″ and viscosity (η) of fully crosslinked HA-Dc are higher than that of incompletely crosslinked HA-Dc (Fig. S8). Based on the results above, it is evident that fully crosslinked HA-Dc exhibits both favorable injectability and retention properties. And 1% HA-Dc hydrogel with a molecular weight of 300 kDa was chosen for subsequent studies.

### 2.2. Decrosslinking property and temperature stability of the HA-Dc hydrogel

Previous literature has noted that disulfide bonds can be cleaved to produce thiols by reduction reactions [60]. Vitamin C (Vit C) plays a critical role in redox reactions and is relatively safe in clinical practice, so it was selected to evaluate the decrosslinking properties of the HA-Dc hydrogel. Rhodamine B was used to observe dye diffusion in the HA-Dc hydrogel after the addition of Vit C (2 mg/mL), which could represent the decrosslinking properties of the HA-Dc hydrogel. The transformation of HA-Dc from a hydrogel to a liquid was observed with the diffusion of the dye over 30 min (Fig. 3a). The G′ value, G″ value and viscosity (η) of the HA-Dc hydrogel decreased with prolonged incubation time (Fig. 3b). The hydrogel-liquid transition time was 5.5 min after Vit C addition, since the G′ value and the G″ value intersected at this time (Fig. 3b), meaning that the HA-Dc hydrogel showed liquid properties after decrosslinking under Vit C treatment.

The mechanism of the hydrogel-liquid transition was verified using DTNB. The HA-Dc hydrogel with the addition of Vit C (HA-Dc + Vit C) showed an obvious absorption peak at 412 nm similar to that of the raw HA-SH material (Fig. 3c), meaning that the disulfide bonds in HA-Dc had been cleaved by Vit C to form sulfhydryl groups. The decrosslinking of the HA-Dc hydrogel was also verified by $^1$H NMR, which displayed similar peaks from –$CH_2$-SH group in both the HA-Dc + Vit C and HA-SH spectra (Fig. S9). The hydrogel-liquid transition was easily induced by Vit C, which could make the *in vivo* degradation of the HA-Dc hydrogel more controllable. The G′, G″ and η values of the HA-Dc hydrogel were stable when the temperature increased from 20 °C to 100 °C (Fig. 3d), which indicated that the HA-Dc hydrogel could maintain steady injectability and tissue stability *in vivo* during the TA procedure.

### 2.3. Biocompatibility of the HA-Dc hydrogel in vitro

The biocompatibility of the HA-Dc hydrogel was evaluated by examining its cytocompatibility and hemocompatibility. HUVECs were used to verify the *in vitro* toxicity of the HA-Dc hydrogel. After 24 h of incubation with the HA-Dc hydrogel, the viabilities of HUVECs were 100.43%, 98.37%, 95.00% and 92.76% with HA-Dc hydrogel concentrations of 2 mg/mL, 5 mg/mL, 10 mg/mL, and 15 mg/mL, respectively ($p > 0.05$, Fig. S10), showing that the hydrogel had negligible cytotoxicity. When the concentration of the HA-Dc hydrogel was 10 mg/mL, the cell viabilities steadily increased over time (Fig. 3e) after 24 h, 48 h, and 72 h of incubation among the different treatment groups. Calcein acetoxymethyl (AM)/propidium iodide (PI) staining did not show any obvious dead cells after 24 h, 48 h, and 72 h of incubation in all groups (Fig. 3f). This indicates that the HA-Dc and HA-Dc + Vit C hydrogels are not cytotoxic, showing that both the HA-Dc hydrogel and decrosslinked HA-SH are cytocompatible.

In addition, an *in vitro* hemolysis test was used to evaluate the hemocompatibility of the HA-Dc hydrogel. When in contact with blood, there was no obvious hemolysis observed in the HA-Dc hydrogel or HA-Dc + Vit C hydrogel groups. The hemolysis rates after treatment with the HA-Dc and HA-Dc + Vit C hydrogels were both lower than 5% (Fig. S11), which is considered highly hemocompatible. These results demonstrated the good biocompatibility of the HA-Dc hydrogel.

### 2.4. In vitro evaluation of the thermal protection offered by the HA-Dc hydrogel

Thermal protection should be the most important requirement for the HA-Dc hydrogel, and we first evaluated its thermal insulation performance in an *in vitro* porcine liver model. The clinically routinely used 5% Glu and the previously reported hydrogel F127 were used for comparison. The excised porcine liver was cut into cylinders with both a diameter and height of 10 mm and then immersed in hydrodissection materials. An RF electrode with an active tip of 7 mm was inserted into the center of each cylinder, and the temperatures at different distances from the margin of the liver cylinder were detected in real time (Fig. 4a). Under the set ablation parameters, ablation zones with a median diameter of 10 mm were achieved, which was essentially consistent with the reference data provided by STARmed. At the margin (0 mm) of the liver cylinder, all sensors in the three materials detected a peak temperature that was nearly or greater than 42 °C during the TA procedure. At temperature sensor distances of 1 mm, 3 mm, and 5 mm, the peak temperatures detected in the HA-Dc groups were 39 °C, 33 °C, and 30 °C, which were close to the values obtained with 5% Glu (39 °C, 33 °C and 29 °C, respectively). However, the temperatures detected in the F127 groups were 42 °C, 36 °C and 33 °C, respectively, which were significantly higher than those in the other two groups (Fig. 4b–c, Fig. S12). Infrared thermography showed similar results. During ablation, the center of each cylinder could reach the highest temperature of 80 °C. The range of high temperatures (≥40 °C) measured in the cylinders immersed in the HA-Dc hydrogel were similar to those measured with 5% Glu, which was lower than those in F127 (Fig. 4d). These results showed that the HA-Dc hydrogel provided thermal protection comparable to that of the routinely used 5% Glu and was better than the F127 hydrogel.

### 2.5. In vivo evaluation of the injectability, retention, degradability and biosafety of the HA-Dc hydrogel

The first *in vivo* assessment of the HA-Dc hydrogel was in a lower limb rabbit model since neuroprotection was chosen to evaluate thermal protection. In this part of the study, the *in vivo* injectability, retention, degradability and biosafety of the HA-Dc hydrogel were evaluated (Fig. 5a), and 5% Glu and F127 were used as comparisons. The sciatic nerve (SN) is located close to the biceps femoris muscle (BFM) anatomically, so the three kinds of hydrodissection materials (HA-Dc hydrogel, 5% Glu, and F127) were injected to separate the SN and BFM to assess their performance *in vivo* under the guidance of ultrasonography (US) (Fig. S13, Video 1-3). When the same volume (1 mL) of each of these 3 hydrodissection materials were injected over 10 s, the HA-Dc

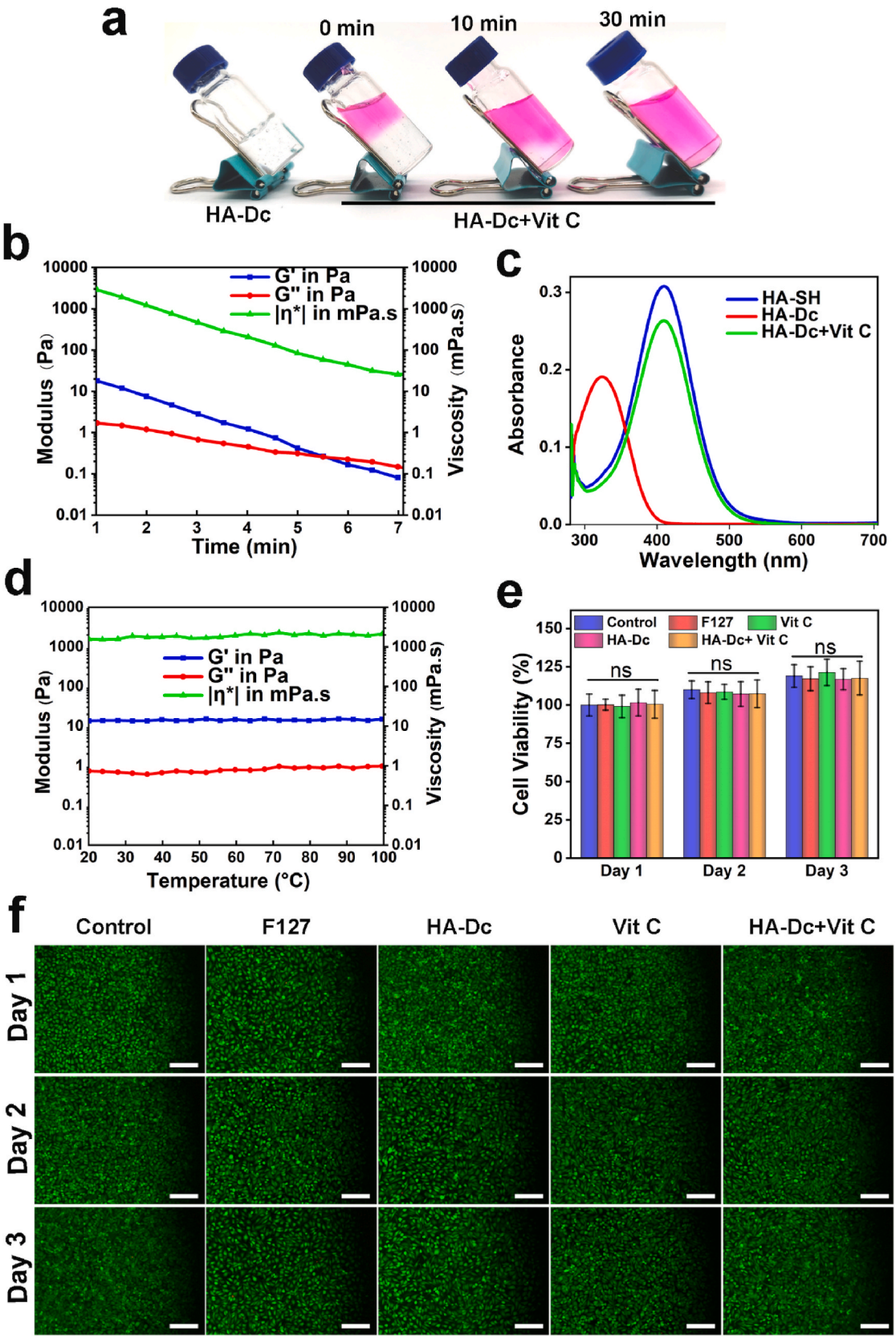


**Fig. 3.** Decrosslinking, temperature stability and biocompatibility characterization of HA-Dc hydrogels *in vitro*. **a** The degradation process of the HA-Dc hydrogel with Vit C (HA-Dc + Vit C) in 30 min **b** Characterization of G′, G″ and η of the HA-Dc hydrogel during the decrosslinking procedure. **c** UV–Vis analysis of HA-SH, HA-Dc and HA-Dc + Vit C. **d** Characterization of G′, G″ and η of HA-Dc hydrogels during the heating process from 20 °C to 100 °C. **e** Cell viability of HUVECs after incubation for 24 h, 48 h, and 72 h with DMEM, F127 (200 mg/mL, the most reported concentration for thermosensitive gelatinization *in vivo*), Vit C (2 mg/mL), HA-Dc (10 mg/mL), and HA-Dc + Vit C (10 mg/mL+2 mg/mL). **f** Calcein AM & PI staining of HUVECs after incubation for 72 h with DMEM, F127 (200 mg/mL), Vit C (2 mg/mL), HA-Dc (10 mg/mL), and HA-Dc + Vit C (10 mg/mL+2 mg/mL). (bar = 5 μm).

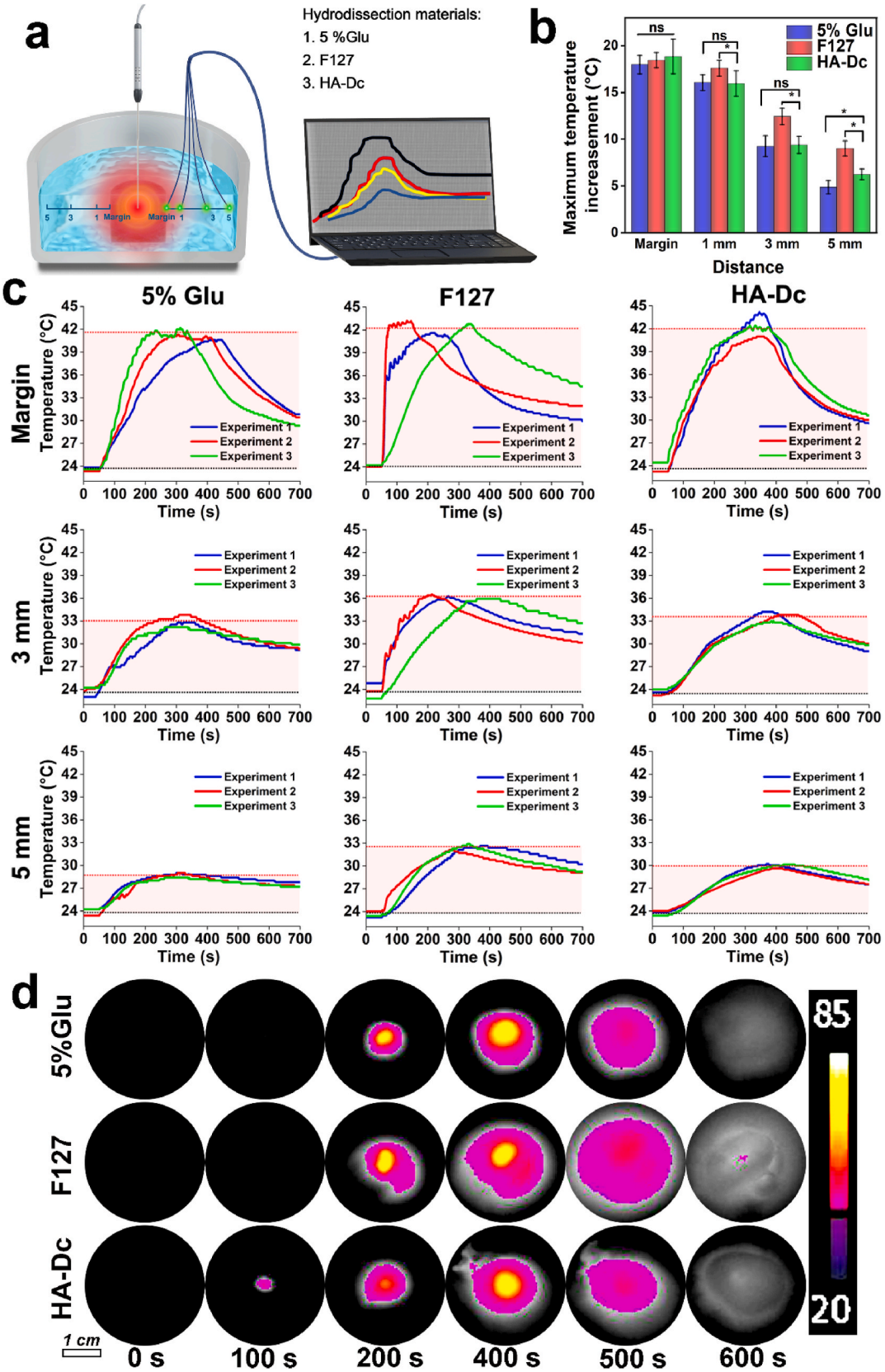


**Fig. 4.** *In vitro* thermal insulation performance validation of the HA-Dc hydrogel. **a** Schematic diagram of the cut liver immersed in hydrodissection materials and temperature monitoring at different distances from the margin of the porcine cylinder during radiofrequency ablation. **b** The maximum temperature increase in the 5% Glu, F127 and HA-Dc hydrogels at the margin (0 mm) and at distances of 1 mm, 3 mm, and 5 mm (n = 3). **c** Temperature curves at the margin (0 mm) at distances of 1 mm, 3 mm, and 5 mm during ablation (n = 3). **d** Infrared thermography of the cur liver immersed in 5% Glu, F127 and HA-Dc hydrogel. (*$p < 0.05$).

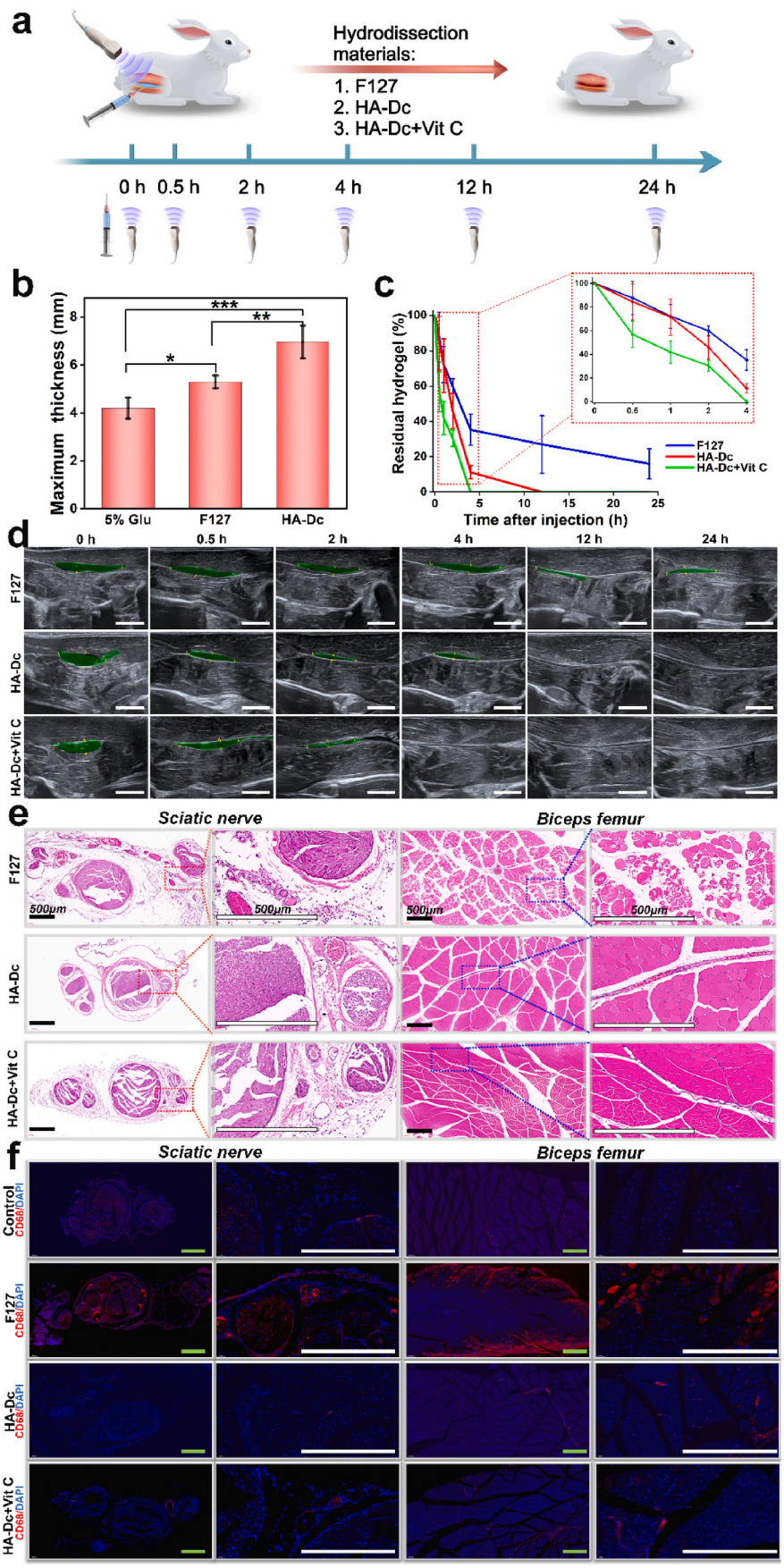


**Fig. 5.** *In vivo* injectability, retention, degradability and biosafety of the HA-Dc hydrogel. **a** Schematic diagram of *in vivo* experiments at the sciatic nerve (SN) and biceps femoris muscle (BFM) of rabbits. **b** The separated distances of SN and BFM after 1 mL 5% Glu, F127, and HA-Dc hydrogel were injected. **c** The volume changes in the hydrodissection in F127, HA-Dc hydrogel and HA-Dc hydrogel with Vit C (HA-Dc + Vit C) over 24 h **d** Degradation procedure on ultrasonography (US). Bar = 1 cm. Yellow arrows: SN; green area, the separated distance by hydrodissection materials. **e** H&E staining and **f** immunofluorescence of cells expressing macrophages (CD68) of SN and BFM 24 h after hydrodissection injection. Bar = 500 μm. (*$p < 0.05$, **$p < 0.01$ and ***$p < 0.001$).

hydrogel achieved the largest separation distance of 7 mm, compared with 5% Glu (4 mm) and F127 (5 mm) (Fig. 5b), indicating that the HA-Dc hydrogel could provide a better separation distance *in vivo* than the other two materials. Subsequent studies revealed that this distance decreased over time. Continued injection of a large amount of 5% Glu was needed to maintain separation during the TA procedure. In comparison, it took 4 h for the distance of separation induced by the HA-Dc hydrogel to decrease to less than 3 mm and 12 h for F127 (Fig. 5c–d), showing that both the HA-Dc hydrogel and F127 had much better retention in the target location to maintain effective separation. In clinical practice, most TA procedures take 1–2 h [61,62], and so effective separation created by the HA-Dc hydrogel that lasts for 4 h is sufficient for the TA procedure. In comparison, the prolonged retention of F127 may cause other side effects and metabolic burden in the body. In addition, the degradation of HA-Dc could be further controlled by adding Vit C according to the TA requirement. Therefore, the degradability of the HA-Dc hydrogel was further evaluated. The HA-Dc hydrogel degraded faster than F127. It took 2 h for HA-Dc + Vit C to decrease to less than 3 mm, and it disappeared on US after 12 h, while F127 could still be visualized by US after 24 h. The addition of Vit C to the HA-Dc hydrogel accelerated its degradability so that the HA-Dc + Vit C hydrogel disappeared on US after 4 h (Fig. 5c–d). The relatively shorter retention time of the HA-Dc hydrogel *in vivo* and its controllable degradability induced by Vit C could help reduce the inflammation caused by the foreign body reaction. The occurrence of this reaction was proven by the histological examination, which showed that although the morphology of the cells in the BFM and SN near all the hydrodissection materials was normal and the SN had a typical myelin structure and standard number of Nissl bodies, the HA-Dc hydrogel and HA-Dc + Vit C produced less inflammatory cell infiltration in the BFM and SN than F127 (Fig. 5e, Fig. S14, Fig. S15). Based on the immunohistochemical analysis of tissue sections as shown in Fig. 5f, macrophages, as typical cells during the acute inflammatory response, were used to analyze the immune reaction with highly expressing of CD68. Compared to the F127 group, the HA-Dc and HA-Dc + Vit C groups exhibited negligible inflammatory cell infiltration, as well as decreased expression of pro-inflammatory cytokines TNF-α and IL-1β (Fig. S16). These findings indicate that HA-Dc showed minimal foreign body reaction, thereby confirming the excellent biocompatibility of HA-Dc hydrogel and HA-Dc + Vit C.

Supplementary video related to this article can be found at https://doi.org/10.1016/j.bioactmat.2023.08.010

The above results demonstrated that the HA-Dc hydrogel could achieve far more separation after injection of a small volume and had sufficient retention in the target location *in vivo* to be effective, which basically solves the current clinical paradox of hydrodissection caused by the good liquidity of 5% Glu and saline. The retention time (4 h) of the HA-Dc hydrogel *in vivo* was essentially suitable for TA, and its degradation *in vivo* could be controlled by Vit C to reduce the metabolic burden and foreign body reaction. These data indicate that according to the demands and complexity of TA procedures, clinicians could meet different thermal protection and controllable degradation demands by adjusting the injected volume of the HA-Dc hydrogel, the time point of Vit C injection, and so on.

### 2.6. *In vivo* evaluation of the HA-Dc hydrogel during BFM ablation in rabbits

Further *in vivo* evaluations of the HA-Dc hydrogel during the TA procedure were carried out with a rabbit BFM ablation model. We focused on thermal protection, the most important requirement for the HA-Dc hydrogel, and we chose neuroprotection as the evaluation index since the nerves are more sensitive to temperature and have a lower temperature threshold at which damage occurs (42 °C) [55,56]. An RF electrode was inserted into the BFM directly (control group) or after the BFM and SN were separated by hydrodissection material (HA-Dc hydrogel, 5% Glu, or F127). According to the thermal ablation guidelines for thyroid nodules, hydrodissection is an essential adjunctive thermal protection technique [57]. During the ablation process, it is generally required to establish a liquid barrier of at least 5 mm around the target area to isolate it from nearby critical structures. Therefore, we adopted a 5 mm isolation band thickness as the standard to determine the volume of injected liquid *in vivo*. In this part, we determined that a separation distance of 5 mm was effective for the following reasons: 1) based on the results from the *in vitro* porcine liver cylinders, at this distance, the peak temperatures in all materials were lower than 35 °C, which could theoretically provide good neuroprotection; and 2) the whole TA procedure, including insertion of the RF electrode and BFM ablation, was monitored by US. The US probe should contact the skin well so that compression of the separated distance is inevitable. An effective ablation time of 1 min on the BFM began with the set ablation parameters, and the real-time temperature at the SN was recorded (Fig. 6a). Among the 3 groups of hydrodissection materials, both HA-Dc hydrogel and F127 produced an effective separation distance after a single injection of only 1 mL, and this distance remained stable before, during and immediately after ablation, showing their good retention in the target locations. In contrast, the effective separation distance in the 5% Glu group could be achieved by only continuous injection of 15 mL of 5% Glu during the whole procedure. The control group showed the highest peak temperatures (43–44 °C) and temperature increase (7 °C) at the SN. The HA-Dc hydrogel group showed peak temperatures of 40–42 °C. Although the peak temperatures in the HA-Dc hydrogel group were slightly higher than those in the 5% Glu group (38–39 °C), the temperatures of the former did not exceed the extreme limit of temperature for nerves (42 °C). The neuroprotection provided by the HA-Dc hydrogel was better than that of F127, which showed peak temperatures near or over 42 °C (Fig. 6b–f).

Immediately after ablation, the same volume of Vit C (1 mL) was injected into the HA-Dc hydrogel, and the separation distance decreased over time. It took 1 h for the distance in the 5% Glu and HA-Dc + Vit C groups to decrease to less than 3 mm on US and 4 h for F127 (Fig. 6g). The HA-Dc + Vit C hydrogel disappeared on US after 4 h, while 5% Glu and F127 still showed small residuals between the BFM and SN at this time point (Fig. 6g). Compared to previous degradation studies, we noticed that the retention time of the F127 hydrogel decreased with RFA treatment, which might be due to the following reasons: 1) the separated distance may be compressed because of the inevitable compression of the US probe during the RFA procedure; and 2) the transition of F127 to the liquid phase (>60 °C) during the RFA procedure affected its retention and nerve protection capability, while the HA-Dc hydrogel showed much better *in vivo* stability from 20 °C to 100 °C (Fig. 3d).

The neuroprotection of these hydrodissection materials was further evaluated by histological examination. Gross evaluations showed significant damage to the SN and BFM in the control group, while there was no obvious damage to the SN in the other groups that used hydrodissection materials during the TA procedure (Fig. S17). The ablated BFM showed evident coagulative necrosis and direct morphological destruction of the muscle cells in all the groups by hematoxylin and eosin (H&E) staining (Fig. 7). The SN showed intact nerve tissues, a normal myelin structure and a typical number of Nissl bodies in the HA-Dc + Vit C and 5% Glu groups, while a broken myelin structure and fewer Nissl bodies were observed in the control and F127 groups (Fig. 7, Fig. S18).

The above results demonstrated that the HA-Dc hydrogel had good retention in the target location, so less of this material could be injected and used to achieve comparative thermal protection of nerves during the rabbit BFM TA procedure. The HA-Dc hydrogel also degraded well after TA, disappearing as quickly as 4 h after the addition of Vit C. This result indicated good controllable degradability after ablation, which is important to avoid possible damage caused by long-term retention in the body.

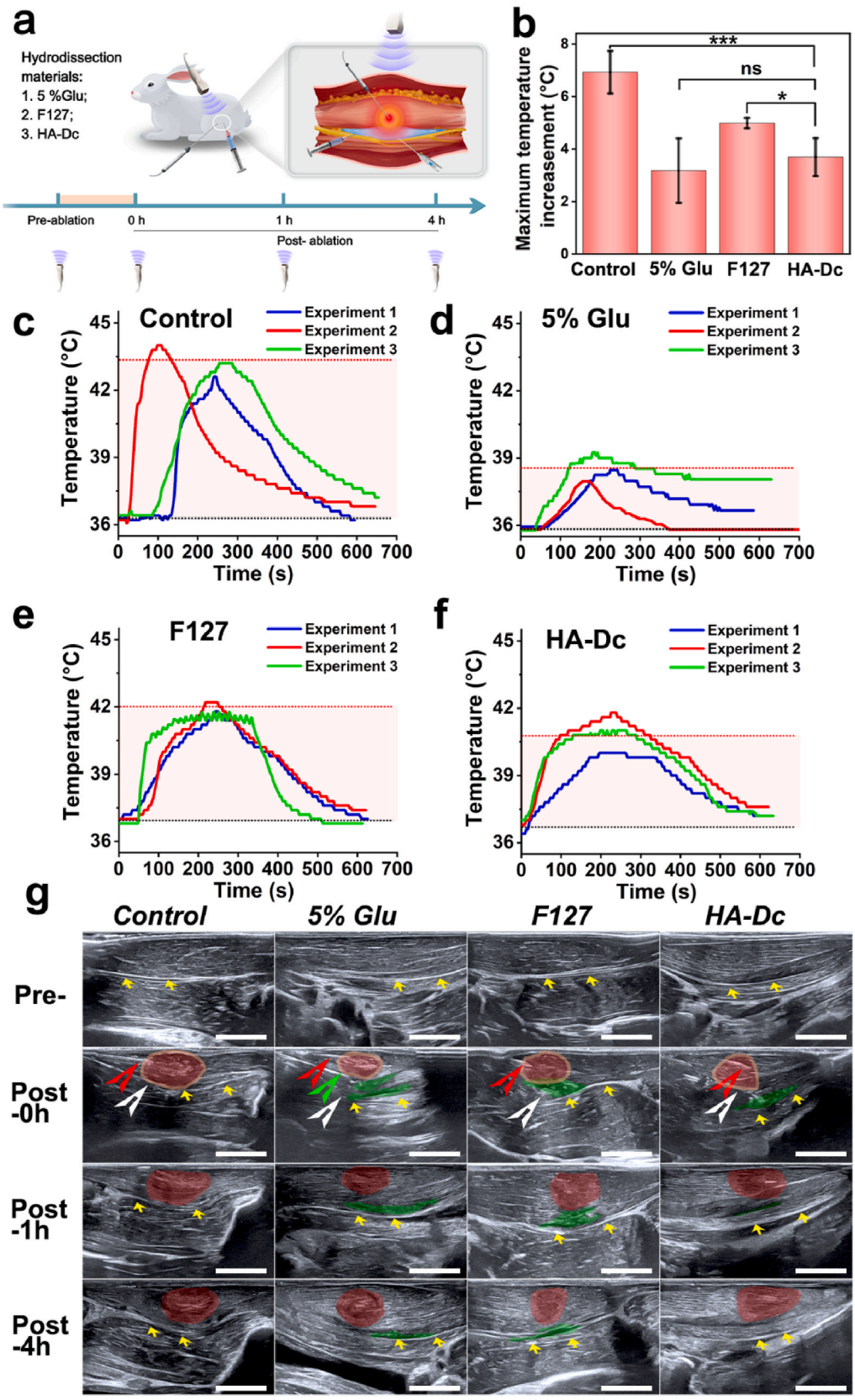


**Fig. 6.** *In vivo* thermal protection of the HA-Dc hydrogel in rabbits. **a** Schematic diagram of *in vivo* thermal protection for the sciatic nerve (SN) when ablation of the biceps femoris muscle (BFM). **b** The maximum temperature increase at the SN of the control, 5% Glu, F127 and HA-Dc hydrogels during ablation on BFM (n = 3). **c-f**. Temperature curves at the SN of control, 5% Glu, F127 and HA-Dc during ablation on BFM (n = 3). **g** Ablation procedure on ultrasonography (US). Bar = 1 cm. Yellow arrows: SN; red arrows: ablation electrode; white arrows: temperature sensor; green arrows: the remaining needle for the continuous injection of 5% Glu; red area, ablation zone in BFM; green area, the separated distance by hydrodissection materials. (*$p < 0.05$, ***$p < 0.001$).

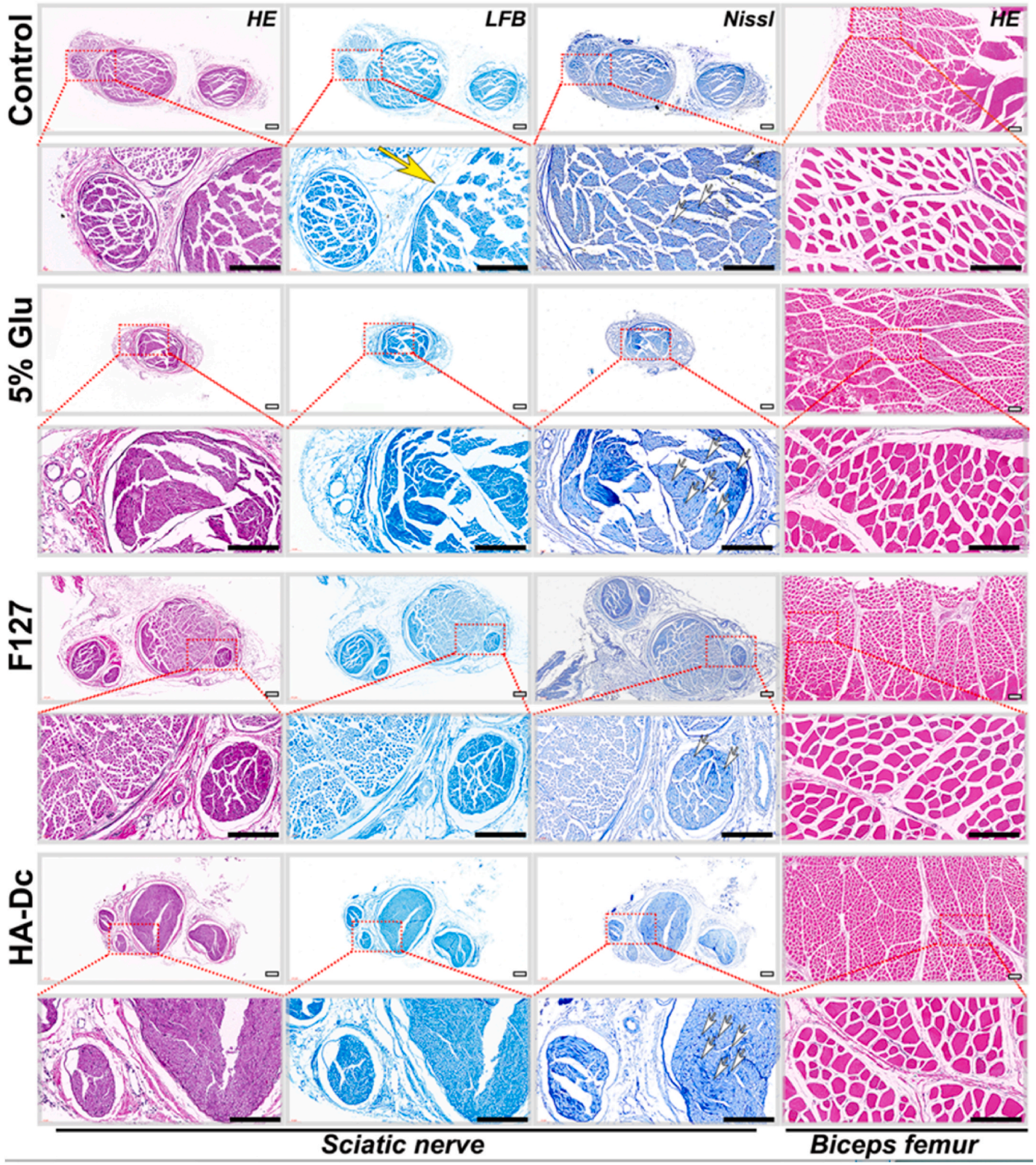


**Fig. 7.** Histological examination of the sciatic nerve (SN) and biceps femoris muscle (BFM) after ablation.

### *2.7. In vivo evaluation of the HA-Dc hydrogel during ablation in M. fascicularis*

According to the above evaluations, the HA-Dc hydrogel had good retention, excellent thermal protection, and controllable degradability in the rabbit model. Thus, this hydrogel shows promising potential for clinical applications, but further verification in animal models that are more similar to the human body is very important and needed. Therefore, in this part, we used primates as a model, as their anatomical structures and physiological status are similar to those of humans, to further evaluate the HA-Dc hydrogel during the TA procedure.

#### *2.7.1. In vivo evaluation of the HA-Dc hydrogel during ablation of the BFM*

The first *in vivo* evaluation of the HA-Dc hydrogel in primates was

performed during ablation of the BFM of *M. fascicularis* (Fig. 8a). In this part, only 5% Glu was used as the comparison to simulate clinical practice. The HA-Dc hydrogel produced an effective separation distance between the BFM and SN after a single injection of only 1 mL, and the separation distance remained stable before, during and immediately after ablation, showing good retention in the target locations (Fig. 8d). In comparison, the effective separation distance was maintained in the 5% Glu group by the continuous injection of 12 mL before and during ablation, but the 5% Glu rapidly disappeared on US immediately after ablation (Fig. 8d). If the 5% Glu injection volume was converted to the dosage needed for a 60 kg adult human, nearly 300 mL of 5% Glu would be needed during ablation to achieve effective separation, which is a very large amount of liquid for the intermuscular space. As shown in Fig. 8b and c, the temperature at the SN rose less in the HA-Dc group than in the 5% Glu group. Notably, the peak temperatures in the HA-Dc hydrogel group were 38–39 °C, which were lower than the critical safe temperature of 42 °C, showing its good thermal protection of nerves.

Immediately after ablation, the same volume of Vit C (1 mL) was injected into the animals in the HA-Dc hydrogel group, and the separated distance decreased over time. It took 1 h for HA-Dc + Vit C to decrease to less than 3 mm on US and it disappeared on US at after 4 h, displaying similar performance to the *in vivo* rabbit model.

There was no significant damage to the SN in either group (HA-Dc hydrogel and 5% Glu) in terms of gross evaluation (Fig. S19). The ablated BFMs in both groups showed evident coagulative necrosis and direct morphological destruction of the muscle cells by H&E staining (Fig. 8e). The SN showed intact nerve tissues and a normal myelin structure in the HA-Dc + Vit C group, while it showed a mildly broken myelin structure in the 5% Glu group (Fig. 8e, Fig. S20, Fig. S21). The possible explanation for this result was that the separation distance provided by 5% Glu would decrease to less than 5 mm during ablation because of its liquidity. Even though 5% Glu was continuously injected, the effective separation distance of 5 mm could not be kept steady during ablation, and unsatisfactory neuroprotection in the TA procedure resulted. In contrast, the HA-Dc hydrogel displayed better thermal protection on SN because of its stable retention. Its controllable degradability induced by Vit C in less than 4 h also helped to avoid possible damage caused by long-term body retention.

#### 2.7.2. *In vivo evaluation of the HA-Dc hydrogel during ablation of the thyroid*

A *M. fascicularis* thyroid ablation model was used to simulate its clinical applicability for TN ablation, where the hydrodissection technique and neuroprotection during the TA procedure are very important. During TA of TNs, hydrodissection materials are usually injected between the thyroid lobe and the recurrent laryngeal nerve (RLN) to separate the thyroid from the surrounding critical structures (e.g., RLN and vagus nerve [VN]) [34]. In this part, 5% Glu was used as the comparison to simulate clinical practice. An RF electrode was inserted into the thyroid lobe after the thyroid and RLN were separated with the HA-Dc hydrogel or 5% Glu, and an effective ablation of the thyroid was carried out for 1 min with the set ablation parameters. The real-time temperature at the RLN was recorded (Fig. 9a).

The HA-Dc hydrogel produced an effective separation distance between the thyroid and RLN after a single injection of only 1 mL, and the separation distance remained stable before, during and immediately after ablation, showing the good retention of the hydrogel in the target locations. In comparison, 5% Glu separated the thyroid and RLN with a maximum distance of only 3 mm. Even with continuous injection of 12 mL, the distance did not reach 5 mm. Immediately after ablation, there was no separation between the thyroid lobe and RLN in the 5% Glu group on US (Fig. 9d). If the 5% Glu injection volume was converted to the dosage needed for a 60 kg adult human, even nearly 300 mL of 5% Glu could not achieve a comparable separation distance. Considering that the cervical spaces are relatively narrow and that there is general agreement that over 50 mL of bleeding in the neck causes airway obstruction in humans [63], some studies have suggested that a small volume of fluid (less than 40 mL) should be used [57,64,65]. Nearly 300 mL of 5% Glu is too much for cervical spaces [42], and here, the HA-Dc hydrogel showed its advantage of good retention so that a small amount could be used to achieve effective separation.

Moreover, the HA-Dc hydrogel also showed excellent thermal protection of the neck nerves in this primate model. The sensors at the RLN detected peak temperatures of 39–40 °C when using the HA-Dc hydrogel for thermal protection, which were lower than the critical safe temperature of 42 °C. In comparison, the peak temperatures at the RLN were 42–46 °C in the 5% Glu group (Fig. 9b–c). The isolation zone produced by the injection of HA-Dc in the ultrasound images is significantly thicker than that of 5% glucose, demonstrating the excellent *in vivo* retention performance and structural stability of HA-Dc during the ablation process (Fig. 9d). This result indicated that the HA-Dc hydrogel had better thermal protection than 5% Glu in this primate thyroid model, which was proven by further histological examination. Gross evaluation showed significant damage to the thyroid and RLN in the 5% Glu group, while there was no significant damage to the RLN in the HA-Dc hydrogel group (Fig. S22). The ablated thyroid showed coagulative necrosis and destruction of the follicular structure in both groups by H&E staining (Fig. 9e). The RLN and VN showed normal myelin structures and a typical number of Nissl bodies in the HA-Dc hydrogel group, while the RLN and VN myelin structures were broken and fewer Nissl bodies were observed in the 5% Glu group (Fig. S23, Fig. S24).

The limited cervical space and good liquidity to easily spread to other potential spaces, such as the mediastinum, could probably explain the unsatisfactory performance of 5% Glu in this experiment. This result indicated the potential advantages of the HA-Dc hydrogel in a narrow space with critical adjacent structures. Its good retention could provide an effective separation distance and further thermal protection of these adjacent structures during the TA procedure.

## 3. Conclusion

In summary, the novel HA-Dc hydrogel designed in our study met all the requirements of ideal hydrodissection materials. It showed good retention, excellent thermal protection even for thermally sensitive nerves, and controllable degradability *in vitro* and *in vivo*, including in primate models, which are more similar to the human body. When compared with the clinically routinely used 5% Glu and the most widely studied hydrogel F127, this novel HA-Dc hydrogel showed prominent advantages. It has promising potential in clinical practice, especially for use in narrow spaces with critical adjacent structures. It can be used in most clinical routine TA procedures, such as for HCC, TNs, and renal tumors. In future studies, this hydrogel might allow the expansion of applying TA to certain restricted parts of the human body, such as pancreatic cancers.

## 4. Materials and methods

### 4.1. Materials

Sodium hyaluronates (HA, molecular weight [$M_w$] = 100 kDa, 300 kDa and 1200 kDa) were purchased from Xi'an Langde Biotechnology Co., Ltd. (China). L-Cystine dimethyl hydrochloride, 1-hydroxybenzotriazole (HOBt), ethyl carbamate, rhodamine B, vitamin C (Vit C), 1-ethyl-3-(3-dimethylaminopropyl) carbodiimide (EDCI), 5,5'-dithiobis-(2-nitrobenzoic acid) (DTNB), and tris-(2-carboxyethyl) phosphine (TCEP) were purchased from Aladdin (China). Dulbecco's modified Eagle's medium (DMEM), fetal bovine serum (FBS), penicillin–streptomycin, and trypsin were purchased from Gibco (Thermo Fisher Scientific, USA). The Calcein acetoxymethyl (AM)/propidium iodide (PI) kit and Cell Counting Kit-8 (CCK-8) were purchased from Meilunbio (China). Triton X-100 was purchased from Beijing Dingguo Changsheng Biotechnology Co., Ltd. (China). Human umbilical vein endothelial cells

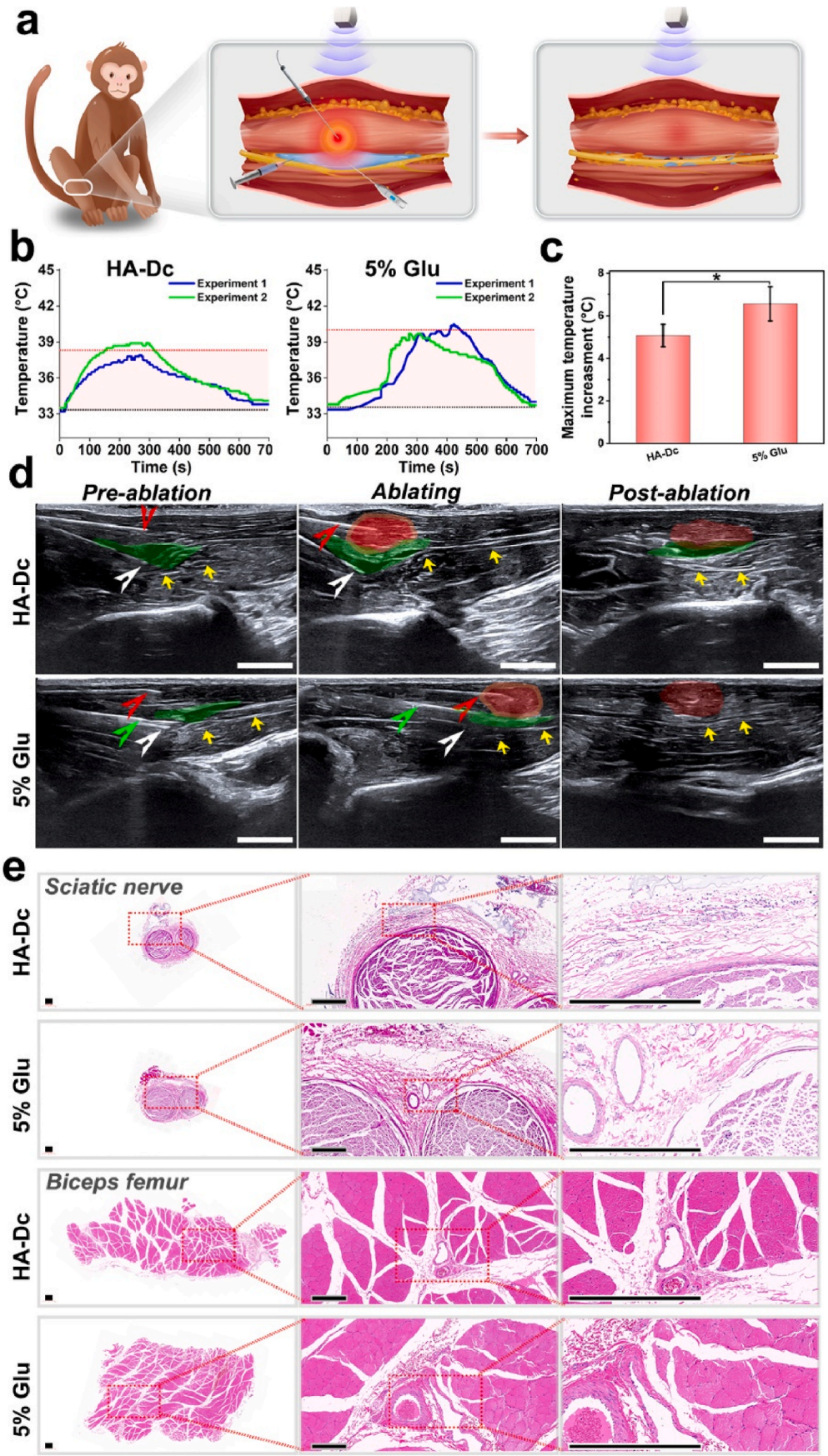


**Fig. 8.** *In vivo* thermal protection of the sciatic nerve (SN) by the HA-Dc hydrogel in *M. fascicularis*. **a** Schematic diagram of *in vivo* thermal protection for SN when ablation on biceps femoris muscle (BFM). **b** Temperature curves at the SN of 5% Glu and HA-Dc hydrogel during ablation on BFM (n = 2). **c** The maximum temperature increase at the SN of 5% Glu and HA-Dc hydrogel during ablation on BFM (n = 2). **d** Ablation procedure on ultrasonography (US). Bar = 1 cm. Yellow arrows: SN; red arrows: ablation electrode; white arrows: temperature sensor; green arrows: the remaining needle for the continuous injection of 5% Glu; red area, ablation zone in BFM; green area, the separated distance by hydrodissection materials. **e** Histological examination of the SN and BFM after ablation (H&E staining). (*$p < 0.05$).

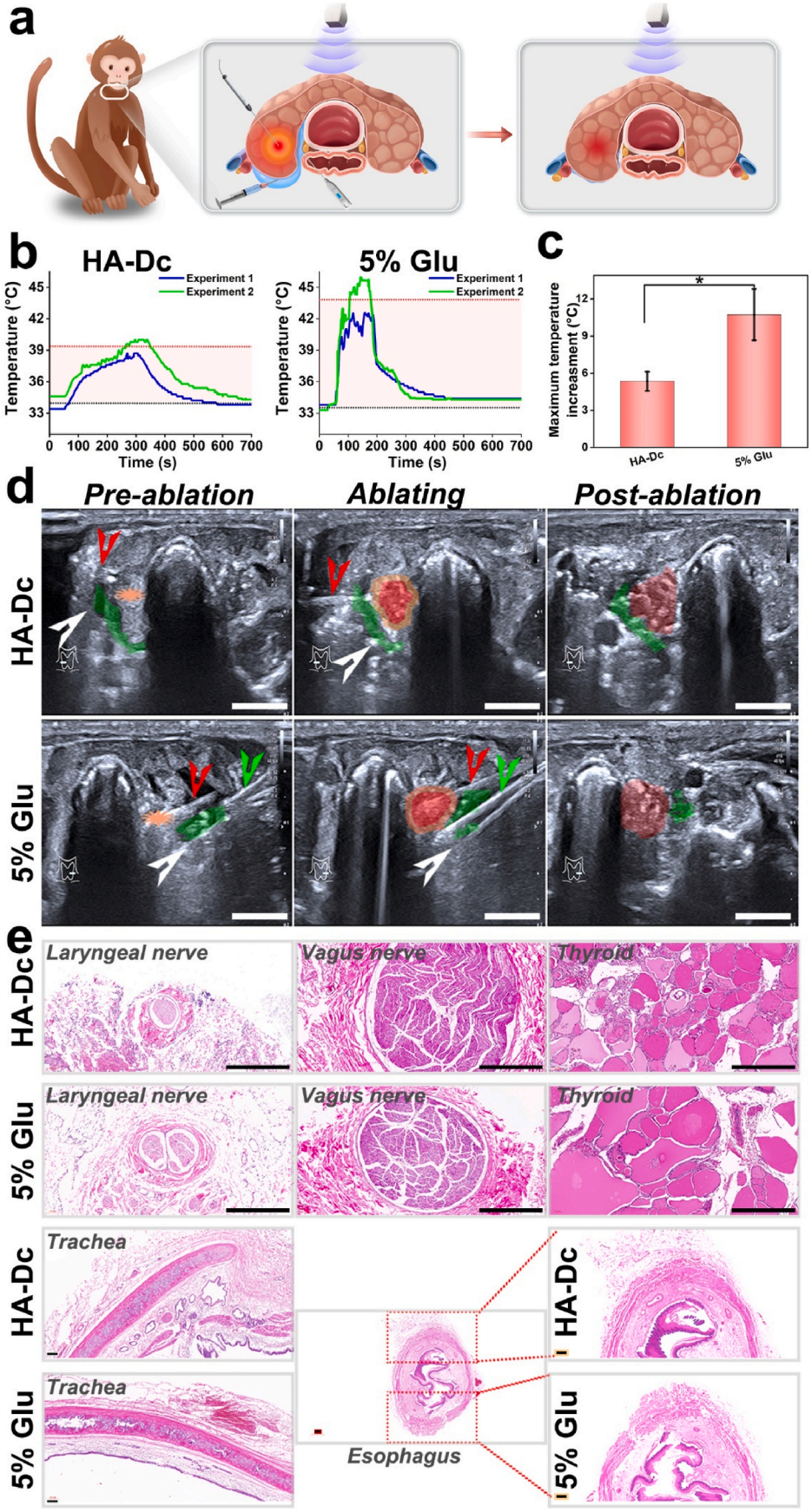


**Fig. 9.** In vivo thermal protection of the HA-Dc hydrogel for the recurrent laryngeal nerve (RLN) and vagus nerve (VN) in *M. fascicularis*. **a** Schematic diagram of *in vivo* thermal protection for the RLN and VN when ablating the thyroid. **b** Temperature curves at the RLN of 5% Glu and HA-Dc hydrogel during ablation of the thyroid (n = 2). **c** The maximum temperature increase at the RLN of 5% Glu and HA-Dc hydrogel during ablation of the thyroid (n = 2). **d** Ablation procedure on ultrasonography (US). Bar = 1 cm. Red arrows: ablation electrode; white arrows: temperature sensor; green arrows: the remaining needle for the continuous injection of 5% Glu; red area, ablation zone in BFM; green area, the separated distance by hydrodissection materials. **e** Histological examination of the thyroid, RLN, VN, esophagus and trachea after ablation (H&E staining). (*$p < 0.05$).

(HUVECs) were purchased from the Chinese Academy of Sciences (China). Deuterium oxide ($D_2O$) and urethan were purchased from Macklin (China). New Zealand rabbits were purchased from Guangdong Medical Laboratory Animal Center (China). *M. fascicularis* and telazol were obtained from Guangdong Landau Biotechnology Co., Ltd. (China). All animals were kept in the Laboratory Animal Center of Sun Yat-sen University. All experimental animal protocols were carried out following the Guangdong Regulations of Laboratory Animal Management and were authorized by the ethics committee of Sun Yat-sen University.

### 4.2. Synthesis of the HA-Dc hydrogel

**Preparation of sulfhydryl hyaluronate (HA-SH).** The entire synthesis was performed under sterile conditions. HA (4.0 g, 10 mmol) was dissolved in 400 mL of sterile water and stirred overnight, and then 1.7 g of L-Cystine dimethyl hydrochloride (5 mmol) was added to the solution, which was stirred until complete dissolution was achieved. Both catalysts, HOBt (2.7 g, 20 mmol) and EDCI (3.8 g, 20 mmol), were mixed into the solution with stirring. TCEP (5.7 g, 20 mmol) was further added for decrosslinking of the disulfide bonds with further stirring for 24 h. The solution was lyophilized and collected after 48 h of dialysis using 12 k-14 kDa dialysis bags to obtain HA-SH.

**Preparation of the hyaluronic acid (HA-Dc) hydrogel.** Lyophilized HA-SH powders with $M_w$ values of 100 kDa, 300 kDa and 1200 kDa were dissolved in 20 mL of sterile water and stirred at a constant temperature of 40 °C for 48 h to obtain HA-Dc hydrogels at a concentration of 1%.

### 4.3. Characterization of the HA-Dc hydrogel

This transformation was verified by evaluating the dissolution of the hydrosoluble dye Rhodamine B in the HA-Dc hydrogel with Vit C addition (HA-Dc + Vit C). HA-Dc (1 mL) was first placed, and then 1 mL Vit C (2 mg/mL) with Rhodamine B (0.1 mg/mL) was added.

The presence of the methyl and thiol groups of HA-SH were confirmed by $^1$H NMR spectroscopy (Avance III, Bruker, Germany) at 298 K at a concentration of 5 mM in $D_2O$, and a Fourier Transform infrared spectrometer (FTIR) (Nicolet 6700, Thermo Scientific, USA) was used to detect the thiol groups of the lyophilized HA-SH powder. For FTIR analysis, 128 scans were obtained with a resolution of 4 $cm^{-1}$ in the wavelength range of 400–4000 $cm^{-1}$. Scanning electron microscopy (SEM, Gemini SEM500, Zeiss, Germany) was used to further analyze the microstructures of the HA-Dc hydrogels with different $M_w$ values. Lyophilized HA-Dc hydrogels with different $M_w$ values were sputtered in a 7 nm gold spray device (Leica EM ACE600, Germany) for SEM analysis.

### 4.4. Viscosity and injectability of the HA-Dc hydrogel

The viscosity of the HA-Dc hydrogel was determined by a rheometer (HAAKE MARS III, Germany), with increasing oscillatory strain from 0.01% to 100% at a constant frequency of 1 Hz to evaluate the linear viscoelastic region (LVR) and increasing shear rate from 0.1 to 100 $s^{-1}$ to evaluate the viscosity (including loss modulus G′, storage modulus G″, and viscosity changes η). To examine the injectability, HA-Dc hydrogels with different $M_w$ values (100 kDa, 300 kDa and 1200 kDa) were injected by using 22 G, 27 G, and 32 G needles, respectively. The injection force was determined by an Instron tester (USA), with the parameters of an inlet flow rate of 0.1 mL/min and a maximum displacement of 6 mm. The force–displacement curves during injection were recorded. Furthermore, the HA-Dc hydrogels with different concentration of 0.5 wt%, 1.0 wt% and 2.0 wt% were studied for selection.

### 4.5. Decrosslinking and temperature stability of the HA-Dc hydrogel

In theory, the disulfide bonds in the HA-Dc hydrogel could be cleaved by an equal volume of Vit C (2 mg/mL), and then the gel-phase HA-Dc hydrogel could become a liquid. This transformation was verified by evaluating the dissolution of the hydrosoluble dye Rhodamine B in the HA-Dc hydrogel with the addition of Vit C (HA-Dc + Vit C). HA-Dc (1 mL) was first placed, and then 1 mL Vit C (2 mg/mL) with Rhodamine B (0.1 mg/mL) were added. The dissolution of Rhodamine B was recorded from initiation to 30 min in 10 min intervals. During the decrosslinking procedure, the viscosity of HA-Dc + Vit C was determined by a rheometer, including the parameters G′, G″, and η. In addition, 0.05 mL of DTNB (4 mg/mL, 0.1 M, pH 8.0) was added to 2 mL of HA-SH, HA-Dc hydrogel, or HA-Dc + Vit C to detect the thiol groups by UV–vis spectroscopy (PerkinElmer LAMBDA35, USA) [33]. The presence of thiol groups in HA-Dc + Vit C was also validated by $^1$H NMR spectroscopy at 298 K at a concentration of 5 mM in $D_2O$.

The viscosity (including G′, G″, and η) of the HA-Dc hydrogel at different temperatures from 20 °C to 100 °C with temperature increase at a rate of 5 °C/min was determined by the rheometer to evaluate the thermal stability of the HA-Dc hydrogel.

### 4.6. Biocompatibility of the HA-Dc hydrogel

**Cell viability test.** The CCK-8 was used to evaluate the cytotoxicity of the HA-Dc hydrogel. HUVECs were cultured in 96-well plates at a density of $1 \times 10^5$ cells/well at 37 °C in a 5% $CO_2$ atmosphere with DMEM supplemented with 10% (v/v) FBS and 1% (v/v) penicillin–streptomycin. After 24 h, 100 μL of 2 mg/mL, 5 mg/mL, 10 mg/mL, and 15 mg/mL HA-Dc hydrogel was added to the wells. After another 24 h, 100 μL of PBS with 10 μL of CCK-8 was added to each well to evaluate cell viability with a microplate reader (SynergyMX, BioTek, USA) at 450 nm. When the concentration of the HA-Dc hydrogel was 10 mg/mL, its effect on cell viability over time was also evaluated. First, 100 μL of 10 mg/mL HA-Dc hydrogel was added to the HUVECs, and after 24 h, 48 h, and 72 h of incubation, CCK-8 was added to evaluate cell viability. In addition, the cytotoxicity of the HA-Dc hydrogel (10 mg/mL) was compared with the cell viability in the control (DMEM only), Vit C (2 mg/mL), HA-Dc + Vit C (10 mg/mL+2 mg/mL), and F127 (200 mg/mL, the most reported concentration for thermosensitive gelatinization *in vivo*) groups.

Calcein-AM/PI staining was also used to compare the cytotoxicity of the HA-Dc hydrogel to that of other materials. HUVECs were cultured in 48-well plates, and DMEM only (control), HA-Dc hydrogels (10 mg/mL), Vit C (2 mg/mL), HA-Dc + Vit C (10 mg/mL+2 mg/mL), or F127 (200 mg/mL) was added. After 24 h, 48 h, and 72 h of incubation, 10 mL of buffer containing 10 μL of Calcein AM and 5 μL of PI was used for cell staining, where Calcein AM was used to stain live cells and PI was used to stain dead cells, to evaluate cell survival with an inverted fluorescence microscope (Olympus IX71, Japan).

**Hemolysis test *in vitro*.** Venous blood samples from New Zealand rabbits were prepared for this test. Before the test, 0.2 mL of HA-Dc hydrogel (10 mg/mL), Vit C (2 mg/mL), HA-Dc + Vit C (10 mg/mL+2 mg/mL), and F127 (200 mg/mL) were dissolved in 2 mL of sterile saline and soaked at 37 °C for 24 h. These materials were mixed with 2.5 mL of sterile saline with 2% venous blood for 3 h of incubation before centrifugation at 1500 rpm for 10 min. The supernatants were collected to evaluate the absorbance values (ABS) using a microplate reader at 540 nm. Triton X-100 and saline were used as the positive and negative controls, respectively, and the hemolysis rate of each material was calculated as follows: hemolysis rate (%) = (ABSsample - ABSnegative)/(ABSpositive- ABSnegative) *100%.

### 4.7. In vitro evaluation of the thermal protection of the HA-Dc hydrogel

The *in vitro* thermal protection of the HA-Dc hydrogel was compared with that provided by 5% glucose (Glu) and F127 in this experiment with excised porcine liver. The porcine liver was cut into cylinders with both a diameter and height of 10 mm by using a surgical skin remover (3

bio Technology Co., Ltd., China). The cylinders were immersed in the HA-Dc hydrogel, 5% Glu or F127. An 18 G RF electrode (STARmed, Korea) with an active tip of 7 mm was inserted into the center of each cylinder. According to the reference data presented by STARmed, this electrode could achieve an ablation zone with a cross-sectional diameter of 10 mm. Temperature sensors (FOTS-MINA-10150-H, INDIGO, China) were set at different distances from the margin of the porcine cylinder (0 mm, 1 mm, 3 mm, and 5 mm) to simultaneously detect the real-time temperatures at different distances during liver cylinder ablation. An infrared thermography detector (E30, FLIR, USA) was also set immediately above the cylinders to record the temperature change during ablation.

The ablation parameters included a pulsed mode, a power output of 40 W, and an effective ablation time of 1 min. Real-time temperature recordings from the sensors started 1 min before ablation and continued until 10 min, and those on the infrared thermography detector started 10 s before ablation and were taken at 60 s intervals until reaching 10 min. The peak temperature and the temperature from the sensors and the highest temperature of the cylinder center and the high temperature range ($\geq$40 °C) from the infrared thermography detector were recorded.

### 4.8. In vivo evaluation of the injectability, retention, degradability, and biosafety of the HA-Dc hydrogel

The first *in vivo* assessment of the HA-Dc hydrogel was in a lower limb rabbit model since neuroprotection was chosen to evaluate thermal protection. To evaluate the retention, degradability, and biosafety of the HA-Dc hydrogel *in vivo*, 12 healthy New Zealand rabbits (2.5–3.0 kg) were included in this study. To evaluate the *in vivo* injectability and retention of the hydrogel, since the sciatic nerve (SN) is located close to the biceps femoris muscle (BFM) anatomically, the hydrodissection materials were injected to separate them to assess their performance *in vivo*. In total, 24 BFMs were included. Following anesthesia with 1 g/kg urethan, a 27 G needle was inserted and placed between the SN and the BFM under the guidance of ultrasonography (US; GE LOGIQ E20, USA). The same volumes (1 mL) of HA-Dc hydrogel (12 BFM), 5% Glu (6 BFM), or F127 (6 BFM) were injected for separation. The separated distance of each group was recorded.

Since there is no need for the HA-Dc hydrogel to stay continuously *in vivo*, the degradability of the HA-Dc hydrogel was further evaluated. In this experiment, 18 BFMs injected with HA-Dc hydrogel and F127 were included. In the 12 BFMs that were injected with the HA-Dc hydrogel, 6 BFMs were injected with Vit C at the same volume (1 mL) as that of the injected HA-Dc hydrogel. The changes in the separation distance in each group were evaluated by US at 30 min, 2 h, 4 h, 12 h and 24 h.

After the last US evaluation, all rabbits were sacrificed. The BFM and SN of each rabbit were sectioned for histological evaluation of biosafety. All samples were embedded in paraffin blocks, sectioned, stained with hematoxylin and eosin (H&E), Luxol Fast Blue (LFB), and toluidine blue, and scanned by an optical microscope (Motic AE31, China).

### 4.9. In vivo evaluation of the HA-Dc hydrogel during biceps femoris muscle (BFM) ablation in rabbits

Further *in vivo* evaluations of the HA-Dc hydrogel during the TA procedure were performed. We focused on thermal protection, the most important requirement for the HA-Dc hydrogel, and we chose neuroprotection as the evaluation index since the nerves are more sensitive a lower temperature threshold at which damage occurs (42 °C) [30]. First, ablation of the BFMs of rabbits was used. Twelve healthy New Zealand rabbits (2.5–3.0 kg) with 24 BFMs were divided into 4 groups: control (no hydrodissection), HA-Dc + Vit C, 5% Glu, and F127 (each group contained 3 rabbits and 6 BFMs). Following anesthesia, a 27 G needle was inserted and placed between the SN and the BFM, and HA-Dc hydrogel, 5% Glu or F127 was injected to separate the BFM and SN to a distance of 5 mm. Then, an 18 G RF electrode with an active tip of 5 mm was inserted into the midst of each BFM, and the temperature sensors were inserted near the SN to detect the real-time temperature during ablation of the BFM. In the HA-Dc + Vit C and F127 groups, the 27 G needle was withdrawn when the initial injection produced a separation distance of 5 mm, while the needle was kept in place for continuous injection in the 5% Glu group to maintain a stable separation distance of 5 mm. The total injection volumes during ablation in each group were recorded.

The ablation parameters included a pulsed mode, a power output of 40 W, and an effective ablation time of 1 min. Real-time temperature recordings from the sensors started 10 s before the ablation and continued until 10 min. After ablation, Vit C at the same volume (1 mL) as that of the injected HA-Dc was injected into the HA-Dc hydrogel in the HA-Dc + Vit C group. The change in volume in the hydrodissection of each group was evaluated by US immediately, and at 1 h and 4 h after ablation.

After the last US evaluation, all rabbits were sacrificed. The BFM and SN of each rabbit were sectioned for histological evaluation according to the same protocol as mentioned above, and the samples were scanned with an optical microscope.

### 4.10. In vivo evaluation of the HA-Dc hydrogel during ablation in M. fascicularis

Two healthy *M. fascicularis* (2.5 kg) were used to further evaluate the thermal protection of HA-Dc *in vivo*. First, ablation of the BFM was studied. Four BFMs were divided into 2 groups: HA-Dc + Vit C and 5% Glu. Following anesthesia with 5 mg/kg telazol, the same procedure was followed for the HA-Dc hydrogel (2 right BFMs) and 5% Glu (2 left BFMs) of injection, ablation, Vit C injection (2 right BFM), and data recording.

Then, to further simulate clinical application, ablation of the thyroid was used since the hydrodissection technique and neuroprotection during TA on thyroid nodules are very important. The 4 thyroid lobes were divided into the same 2 groups (HA-Dc + Vit C and 5% Glu), and a 27 G needle was inserted and placed between the thyroid lobe and the recurrent laryngeal nerve (RLN). The HA-Dc hydrogel (2 right lobes) or 5% Glu (2 left lobes) was injected to separate the lobes and the surrounding critical structures, including the RLN, vagus nerve (VN), esophagus, and trachea. Then, an 18 G RF electrode with an active tip of 5 mm was inserted into the midst of each lobe, and the temperature sensors were inserted near the RLN to detect the temperature in real time during ablation of the thyroid. In the HA-Dc + Vit C group, the 27 G needle was withdrawn when the initial injection produced a separation distance of 5 mm, while the needle was kept in place for continuous injection in the 5% Glu group to maintain a stable separation distance of 5 mm. The total injection volumes during ablation in each group were recorded. The same ablation parameters were used. Real-time temperature recordings from the sensors started 10 s before ablation and continued for 10 min. After ablation, Vit C at the same volume (1 mL) as that of the injected HA-Dc was injected into the HA-Dc hydrogel in the HA-Dc + Vit C group. The change in volume of the hydrodissection in each group was evaluated by US immediately and at 1 h and 4 h after ablation.

After the last US evaluation, both *M. fascicularis* were sacrificed. The BFM, SN, thyroid, RLN, VN, trachea, and esophagus of each *M. fascicularis* were sectioned for histological evaluation with the same protocol as mentioned above and scanned by an optical microscope.

### 4.11. Statistical analysis

All data are presented as mean ± standard deviation and analyzed using the Student's t-test or one-way analysis of variance. *p*-values <0.05 was considered statistically significance ($^{*}p < 0.05$, $^{**}p < 0.01$, $^{***}p < 0.001$).

## Ethics approval and consent to participate

All the animal experiments of rabbits were approved by the Institutional Animal Care and Use Committee (IACUC), Sun Yat-Sen University (Approval No.: SYSU-IACUC-2022-001120). All the animal experiments of *M. fascicularis* were approved by the Institutional Animal Care and Use Committee (IACUC), Landau Bio Co. Ltd. (Approval No.: LDACU 20220622–01).

## Declaration of competing interest

The authors declare that they have no known competing financial interests or personal relationships that could have appeared to influence the work.

## CRediT authorship contribution statement

**Bowen Zheng:** Methodology, Validation, Formal analysis, Investigation, Data curation, Writing – original draft, Writing – review & editing. **Peng Zhang:** Methodology, Validation, Formal analysis, Investigation, Data curation, Writing – original draft, Writing – review & editing. **Qijun Lv:** Methodology, Validation, Investigation, Visualization. **Tao Wu:** Methodology, Investigation. **Yadong Liu:** Methodology, Investigation. **Junjie Tang:** Methodology, Investigation. **Yanping Ma:** Methodology, Investigation. **Lili Cheng:** Methodology, Investigation. **Langtao Xu:** Methodology, Investigation. **Yizhen Wang:** Methodology, Investigation. **Yifan Xue:** Methodology, Investigation. **Jie Liu:** Conceptualization, Writing – review & editing, Supervision, Project administration, Funding acquisition. **Jie Ren:** Conceptualization, Writing – review & editing, Supervision, Project administration, Funding acquisition.

## Acknowledgements

This work was financially supported by the National Natural Science Foundation of China (81971632, 51773231), the Natural Science Foundation of Guangdong Province (2020A1515010425, 2022A1515010024), Key Scientific and Technological Program of Guangzhou City (201802020023), and Shenzhen Science and Technology Project (JCYJ20190807160801664, JCYJ20220818103207016).

## Appendix A. Supplementary data

Supplementary data to this article can be found online at https://doi.org/10.1016/j.bioactmat.2023.08.010.

## References

[1] H. Webb, M.G. Lubner, J.L. Hinshaw, Thermal ablation, Semin. Roentgenol. 46 (2) (2011) 133–141, https://doi.org/10.1053/j.ro.2010.08.002.
[2] K.F. Chu, D.E. Dupuy, Thermal ablation of tumours: biological mechanisms and advances in therapy, Nat. Rev. Cancer 14 (3) (2014) 199–208, https://doi.org/10.1038/nrc3672.
[3] N. Vietti Violi, R. Duran, B. Guiu, J.P. Cercueil, C. Aubé, A. Digklia, et al., Efficacy of microwave ablation versus radiofrequency ablation for the treatment of hepatocellular carcinoma in patients with chronic liver disease: a randomised controlled phase 2 trial, Lancet Gastroenterol. Hepatol. 3 (5) (2018) 317–325, https://doi.org/10.1016/s2468-1253(18)30029-3.
[4] N. Gennaro, S. Schiaffino, G. Mauri, L. Monfardini, The what, the why, and the how of liver ablations: a practical guide for the medical oncologist, Oncology 99 (11) (2021) 722–731, https://doi.org/10.1159/000518358.
[5] H. Lee, G.Y. Jin, Y.M. Han, G.H. Chung, Y.C. Lee, K.S. Kwon, et al., Comparison of survival rate in primary non-small-cell lung cancer among elderly patients treated with radiofrequency ablation, surgery, or chemotherapy, Cardiovasc. Intervent. Radiol. 35 (2) (2012) 343–350, https://doi.org/10.1007/s00270-011-0194-y.
[6] X. Ye, W. Fan, Z. Wang, J. Wang, H. Wang, L. Niu, et al., Clinical practice guidelines on image-guided thermal ablation of primary and metastatic lung tumors (2022 edition), J. Cancer Res. Therapeut. 18 (5) (2022) 1213–1230, https://doi.org/10.4103/jcrt.jcrt_880_22.
[7] B.K. Park, S.H. Shen, M. Fujimori, Y. Wang, Asian Conference on Tumor Ablation guidelines for renal cell carcinoma, Invest. Clin. Urol. 62 (4) (2021) 378–388, https://doi.org/10.4111/icu.20210168.
[8] M.R. Moynagh, A.N. Kurup, M.R. Callstrom, Thermal ablation of bone metastases, Semin. Intervent. Radiol. 35 (4) (2018) 299–308, https://doi.org/10.1055/s-0038-1673422.
[9] S.R. Chung, C.H. Suh, J.H. Baek, H.S. Park, Y.J. Choi, J.H. Lee, Safety of radiofrequency ablation of benign thyroid nodules and recurrent thyroid cancers: a systematic review and meta-analysis, Int. J. Hyperther. 33 (8) (2017) 920–930, https://doi.org/10.1080/02656736.2017.1337936.
[10] E.J. Ha, J.H. Baek, Y. Che, Y.H. Chou, N. Fukunari, J.H. Kim, et al., Radiofrequency ablation of benign thyroid nodules: recommendations from the Asian conference on tumor ablation task force, Ultrasonography 40 (1) (2021) 75–82, https://doi.org/10.14366/usg.20112.
[11] M. Mendiratta-Lala, D.D. Brennan, O.R. Brook, S. Faintuch, P.M. Mowschenson, R. G. Sheiman, et al., Efficacy of radiofrequency ablation in the treatment of small functional adrenal neoplasms, Radiology 258 (1) (2011) 308–316, https://doi.org/10.1148/radiol.10100690.
[12] B.K. Park, M. Fujimori, S.H. Shen, U. Pua, Asian conference on tumor ablation guidelines for adrenal tumor ablation, Endocrinol Metab (Seoul). 36 (3) (2021) 553–563, https://doi.org/10.3803/EnM.2021.1008.
[13] C.S. Kaufman, B. Bachman, P.J. Littrup, M. White, K.A. Carolin, L. Freman-Gibb, et al., Office-based ultrasound-guided cryoablation of breast fibroadenomas, Am. J. Surg. 184 (5) (2002) 394–400, https://doi.org/10.1016/s0002-9610(02)01010-3.
[14] R. Geoghegan, G. Ter Haar, K. Nightingale, L. Marks, S. Natarajan, Methods of monitoring thermal ablation of soft tissue tumors - a comprehensive review, Med. Phys. 49 (2) (2022) 769–791, https://doi.org/10.1002/mp.15439.
[15] J.P. McGahan, J.M. Brock, H. Tesluk, W.Z. Gu, P. Schneider, P.D. Browning, Hepatic ablation with use of radio-frequency electrocautery in the animal model, J. Vasc. Intervent. Radiol. 3 (2) (1992) 291–297, https://doi.org/10.1016/s1051-0443(92)72028-4.
[16] M. Ahmed, C.L. Brace, F.T. Lee Jr., S.N. Goldberg, Principles of and advances in percutaneous ablation, Radiology 258 (2) (2011) 351–369, https://doi.org/10.1148/radiol.10081634.
[17] S.N. Goldberg, G.S. Gazelle, P.R. Mueller, Thermal ablation therapy for focal malignancy: a unified approach to underlying principles, techniques, and diagnostic imaging guidance, AJR Am. J. Roentgenol. 174 (2) (2000) 323–331, https://doi.org/10.2214/ajr.174.2.1740323.
[18] R. Lencioni, T. de Baere, R.C. Martin, C.W. Nutting, G. Narayanan, Image-guided ablation of malignant liver tumors: recommendations for clinical validation of novel thermal and non-thermal technologies - a western perspective, Liver Cancer 4 (4) (2015) 208–214, https://doi.org/10.1159/000367747.
[19] S.H. Guan, H. Wang, D.K. Teng, Comparison of ultrasound-guided thermal ablation and conventional thyroidectomy for benign thyroid nodules: a systematic review and meta-analysis, Int. J. Hyperther. 37 (1) (2020) 442–449, https://doi.org/10.1080/02656736.2020.1758802.
[20] L. Xie, H. Qi, F. Cao, L. Shen, S. Chen, Y. Wu, et al., Comparison between surgery and thermal ablation for adrenal metastases: a retrospective study, Int. J. Hyperther. 38 (1) (2021) 1541–1547, https://doi.org/10.1080/02656736.2021.1993356.
[21] H. Nishikawa, T. Inuzuka, H. Takeda, J. Nakajima, F. Matsuda, A. Sakamoto, et al., Comparison of percutaneous radiofrequency thermal ablation and surgical resection for small hepatocellular carcinoma, BMC Gastroenterol. 11 (2011) 143, https://doi.org/10.1186/1471-230x-11-143.
[22] K. Katsanos, L. Mailli, M. Krokidis, A. McGrath, T. Sabharwal, A. Adam, Systematic review and meta-analysis of thermal ablation versus surgical nephrectomy for small renal tumours, Cardiovasc. Intervent. Radiol. 37 (2) (2014) 427–437, https://doi.org/10.1007/s00270-014-0846-9.
[23] A.R. Gillams, W.R. Lees, Five-year survival in 309 patients with colorectal liver metastases treated with radiofrequency ablation, Eur. Radiol. 19 (5) (2009) 1206–1213, https://doi.org/10.1007/s00330-008-1258-5.
[24] J. Palussière, M. Canella, F. Cornelis, V. Catena, E. Descat, V. Brouste, et al., Retrospective review of thoracic neural damage during lung ablation - what the interventional radiologist needs to know about neural thoracic anatomy, Cardiovasc. Intervent. Radiol. 36 (6) (2013) 1602–1613, https://doi.org/10.1007/s00270-013-0597-z.
[25] J.H. Baek, J.H. Lee, J.Y. Sung, J.I. Bae, K.T. Kim, J. Sim, et al., Complications encountered in the treatment of benign thyroid nodules with US-guided radiofrequency ablation: a multicenter study, Radiology 262 (1) (2012) 335–342, https://doi.org/10.1148/radiol.11110416.
[26] C. Kim, J.H. Lee, Y.J. Choi, W.B. Kim, T.Y. Sung, J.H. Baek, Complications encountered in ultrasonography-guided radiofrequency ablation of benign thyroid nodules and recurrent thyroid cancers, Eur. Radiol. 27 (8) (2017) 3128–3137, https://doi.org/10.1007/s00330-016-4690-y.
[27] A. Philip, S. Gupta, K. Ahrar, A.L. Tam, A spectrum of nerve injury after thermal ablation: a report of four cases and review of the literature, Cardiovasc. Intervent. Radiol. 36 (5) (2013) 1427–1435, https://doi.org/10.1007/s00270-012-0491-0.
[28] F. De Muzio, C. Cutolo, F. Dell'Aversana, F. Grassi, L. Ravo, M. Ferrante, et al., Complications after thermal ablation of hepatocellular carcinoma and liver metastases: imaging findings, Diagnostics 12 (5) (2022), https://doi.org/10.3390/diagnostics12051151.
[29] T. Livraghi, L. Solbiati, M.F. Meloni, G.S. Gazelle, E.F. Halpern, S.N. Goldberg, Treatment of focal liver tumors with percutaneous radio-frequency ablation: complications encountered in a multicenter study, Radiology 226 (2) (2003) 441–451, https://doi.org/10.1148/radiol.2262012198.

[30] M.J. Howenstein, K.T. Sato, Complications of radiofrequency ablation of hepatic, pulmonary, and renal neoplasms, Semin. Intervent. Radiol. 27 (3) (2010) 285–295, https://doi.org/10.1055/s-0030-1261787.
[31] C.C. Wang, J.H. Kao, Artificial ascites is feasible and effective for difficult-to-ablate hepatocellular carcinoma, Hepatol. Int. 9 (4) (2015) 514–519, https://doi.org/10.1007/s12072-015-9639-8.
[32] I. Song, H. Rhim, H.K. Lim, Y.S. Kim, D. Choi, Percutaneous radiofrequency ablation of hepatocellular carcinoma abutting the diaphragm and gastrointestinal tracts with the use of artificial ascites: safety and technical efficacy in 143 patients, Eur. Radiol. 19 (11) (2009) 2630–2640, https://doi.org/10.1007/s00330-009-1463-x.
[33] J.W. Kim, S.S. Shin, S.H. Heo, J.H. Hong, H.S. Lim, H.J. Seon, et al., Ultrasound-guided percutaneous radiofrequency ablation of liver tumors: how we do it safely and completely, Korean J. Radiol. 16 (6) (2015) 1226–1239, https://doi.org/10.3348/kjr.2015.16.6.1226.
[34] H.S. Park, J.H. Baek, A.W. Park, S.R. Chung, Y.J. Choi, J.H. Lee, Thyroid radiofrequency ablation: updates on innovative devices and techniques, Korean J. Radiol. 18 (4) (2017) 615–623, https://doi.org/10.3348/kjr.2017.18.4.615.
[35] X. Buy, C.H. Tok, D. Szwarc, G. Bierry, A. Gangi, Thermal protection during percutaneous thermal ablation procedures: interest of carbon dioxide dissection and temperature monitoring, Cardiovasc. Intervent. Radiol. 32 (3) (2009) 529–534, https://doi.org/10.1007/s00270-009-9524-8.
[36] S. Kariya, N. Tanigawa, H. Kojima, A. Komemushi, Y. Shomura, Y. Ueno, et al., Radiofrequency ablation combined with CO2 injection for treatment of retroperitoneal tumor: protecting surrounding organs against thermal injury, AJR Am. J. Roentgenol. 185 (4) (2005) 890–893, https://doi.org/10.2214/ajr.04.1220.
[37] K. Yamakado, A. Nakatsuka, M. Akeboshi, K. Takeda, Percutaneous radiofrequency ablation of liver neoplasms adjacent to the gastrointestinal tract after balloon catheter interposition, J. Vasc. Intervent. Radiol. 14 (9 Pt 1) (2003) 1183–1186, https://doi.org/10.1097/01.rvi.0000086530.86489.05.
[38] A. Froemming, T. Atwell, M. Farrell, M. Callstrom, B. Leibovich, W. Charboneau, Probe retraction during renal tumor cryoablation: a technique to minimize direct ureteral injury, J. Vasc. Intervent. Radiol. 21 (1) (2010) 148–151, https://doi.org/10.1016/j.jvir.2009.09.014.
[39] G. Mauri, L. Nicosia, G.M. Varano, G. Bonomo, P. Della Vigna, L. Monfardini, et al., Tips and tricks for a safe and effective image-guided percutaneous renal tumour ablation, Insights Imag. 8 (3) (2017) 357–363, https://doi.org/10.1007/s13244-017-0555-4.
[40] M.F. Meloni, J. Chiang, P.F. Laeseke, C.F. Dietrich, A. Sannino, M. Solbiati, et al., Microwave ablation in primary and secondary liver tumours: technical and clinical approaches, Int. J. Hyperther. 33 (1) (2017) 15–24, https://doi.org/10.1080/02656736.2016.1209694.
[41] J. Garnon, R.L. Cazzato, J. Caudrelier, M. Nouri-Neuville, P. Rao, E. Boatta, et al., Adjunctive thermoprotection during percutaneous thermal ablation procedures: review of current techniques, Cardiovasc. Intervent. Radiol. 42 (3) (2019) 344–357, https://doi.org/10.1007/s00270-018-2089-7.
[42] Y. Ma, T. Wu, Z. Yao, B. Zheng, L. Tan, G. Tong, et al., Continuous, large-volume hydrodissection to protect delicate structures around the thyroid throughout the radiofrequency ablation procedure, Eur. Thyroid J. 10 (6) (2021) 495–503, https://doi.org/10.1159/000519625.
[43] Y. Kondo, H. Yoshida, S. Shiina, R. Tateishi, T. Teratani, M. Omata, Artificial ascites technique for percutaneous radiofrequency ablation of liver cancer adjacent to the gastrointestinal tract, Br. J. Surg. 93 (10) (2006) 1277–1282, https://doi.org/10.1002/bjs.5374.
[44] B.W. Zheng, T. Wu, Z.C. Yao, Y.P. Ma, J. Ren, Perithyroidal hemorrhage caused by hydrodissection during radiofrequency ablation for benign thyroid nodules: two case reports, World J. Clin. Cases 10 (29) (2022) 10755–10762, https://doi.org/10.12998/wjcc.v10.i29.10755.
[45] L. Jiang, V. Krishnasamy, G.M. Varano, B.J. Wood, Hyponatremia following high-volume D5W hydrodissection during thermal ablation, Cardiovasc. Intervent. Radiol. 39 (1) (2016) 146–149, https://doi.org/10.1007/s00270-015-1195-z.
[46] T. Hasegawa, H. Takaki, H. Miyagi, A. Nakatsuka, J. Uraki, T. Yamanaka, et al., Hyaluronic acid gel injection to prevent thermal injury of adjacent gastrointestinal tract during percutaneous liver radiofrequency ablation, Cardiovasc. Intervent. Radiol. 36 (4) (2013) 1144–1146, https://doi.org/10.1007/s00270-013-0546-x.
[47] A. Johnson, A. Sprangers, P. Cassidy, S. Heyrman, J.L. Hinshaw, M. Lubner, et al., Design and validation of a thermoreversible material for percutaneous tissue hydrodissection, J. Biomed. Mater. Res. B Appl. Biomater. 101 (8) (2013) 1400–1409, https://doi.org/10.1002/jbm.b.32959.
[48] J.J. Fu, S. Wang, W. Yang, W. Gong, A.N. Jiang, K. Yan, et al., Protective and heat retention effects of thermo-sensitive basement membrane extract (matrigel) in hepatic radiofrequency ablation in an experimental animal study, Cardiovasc. Intervent. Radiol. 40 (7) (2017) 1077–1085, https://doi.org/10.1007/s00270-017-1617-1.
[49] L. Huang, S. Yang, M. Bai, Y. Lin, X. Chen, G. Li, et al., Thermal shielding performance of self-healing hydrogel in tumor thermal ablation, Colloids Surf. B Biointerfaces 213 (2022), 112382, https://doi.org/10.1016/j.colsurfb.2022.112382.
[50] D. Zhang, D. Xie, X. Wei, D. Zhang, M. Chen, X. Yu, et al., Microwave ablation of the liver abutting the stomach: insulating effect of a chitosan-based thermosensitive hydrogel, Int. J. Hyperther. 30 (2) (2014) 126–133, https://doi.org/10.3109/02656736.2013.874048.
[51] A.J. Moreland, M.G. Lubner, T.J. Ziemlewicz, D.R. Kitchin, J.L. Hinshaw, A. D. Johnson, et al., Evaluation of a thermoprotective gel for hydrodissection during percutaneous microwave ablation: in vivo results, Cardiovasc. Intervent. Radiol. 38 (3) (2015) 722–730, https://doi.org/10.1007/s00270-014-1008-9.
[52] L.L. Zhang, G.M. Xia, Y.J. Liu, R. Dou, J. Eisenbrey, J.B. Liu, et al., Effect of a poloxamer 407-based thermosensitive gel on minimization of thermal injury to diaphragm during microwave ablation of the liver, World J. Gastroenterol. 23 (12) (2017) 2141–2148, https://doi.org/10.3748/wjg.v23.i12.2141.
[53] A. Johnson, C. Brace, Heat transfer within hydrodissection fluids: an analysis of thermal conduction and convection using liquid and gel materials, Int. J. Hyperther. 31 (5) (2015) 551–559, https://doi.org/10.3109/02656736.2015.1037799.
[54] E.A. Pec, Z.G. Wout, T.P. Johnston, Biological activity of urease formulated in poloxamer 407 after intraperitoneal injection in the rat, J Pharm Sci 81 (7) (1992) 626–630, https://doi.org/10.1002/jps.2600810707.
[55] R. Lecigne, R.L. Cazzato, D. Dalili, A. Gangi, J. Garnon, Transosseous temperature monitoring of the anterior epidural space during thermal ablation in the thoracic spine, Cardiovasc. Intervent. Radiol. 44 (6) (2021) 982–987, https://doi.org/10.1007/s00270-021-02771-y.
[56] R.J. Podhajsky, Y. Sekiguchi, S. Kikuchi, R.R. Myers, The histologic effects of pulsed and continuous radiofrequency lesions at 42 degrees C to rat dorsal root ganglion and sciatic nerve, Spine 30 (9) (2005) 1008–1013, https://doi.org/10.1097/01.brs.0000161005.31398.58.
[57] J.H. Kim, J.H. Baek, H.K. Lim, H.S. Ahn, S.M. Baek, Y.J. Choi, et al., 2017 thyroid radiofrequency ablation guideline: Korean society of thyroid radiology, Korean J. Radiol. 19 (4) (2018) 632–655, https://doi.org/10.3348/kjr.2018.19.4.632.
[58] M. Nikfarjam, V. Muralidharan, C. Christophi, Mechanisms of focal heat destruction of liver tumors, J. Surg. Res. 127 (2) (2005) 208–223, https://doi.org/10.1016/j.jss.2005.02.009.
[59] C. Brace, Thermal tumor ablation in clinical use, IEEE Pulse 2 (5) (2011) 28–38, https://doi.org/10.1109/mpul.2011.942603.
[60] C.E. Paulsen, K.S. Carroll, Cysteine-mediated redox signaling: chemistry, biology, and tools for discovery, Chem. Rev. 113 (7) (2013) 4633–4679, https://doi.org/10.1021/cr300163e.
[61] P. Dong, X.L. Wu, G.Q. Sui, Q. Luo, J.R. Du, H. Wang, et al., The efficacy and safety of microwave ablation versus lobectomy for the treatment of benign thyroid nodules greater than 4 cm, Endocrine 71 (1) (2021) 113–121, https://doi.org/10.1007/s12020-020-02338-w.
[62] T. Wu, B. Zheng, L. Tan, T. Yin, Y. Lian, S. Xu, et al., A novel parallel overlapping mode for complete ablation of large benign thyroid nodules in a single-session radiofrequency ablation, Front. Endocrinol. 13 (2022), 915303, https://doi.org/10.3389/fendo.2022.915303.
[63] H.S. Lee, B.J. Lee, S.W. Kim, Y.W. Cha, Y.S. Choi, Y.H. Park, et al., Patterns of post-thyroidectomy hemorrhage, Clin. Exp. Otorhinolaryngol. 2 (2) (2009) 72–77, https://doi.org/10.3342/ceo.2009.2.2.72.
[64] F. Morelli, A.M. Ierardi, G. Pompili, A. Sacrini, P. Biondetti, S.A. Angileri, et al., Cooled tip radiofrequency ablation of benign thyroid nodules: preliminary experience with two different devices, Gland Surg. 7 (2) (2018) 67–79, https://doi.org/10.21037/gs.2017.11.01.
[65] Y. Zhu, M. Zhang, Z. Jin, X. Tian, Y. Zhang, F. Xie, et al., Solid benign thyroid nodules (>10 ml): a retrospective study on the efficacy and safety of sonographically guided ethanol ablation combined with radiofrequency ablation, Int. J. Hyperther. 37 (1) (2020) 157–167, https://doi.org/10.1080/02656736.2020.1717647.